Key Points:
- Normalized excess mixing ratios of nitrogen species are reported for western U.S. wildfires; median of 66% of emissions are in reduced form
- Within minutes after emission, rapid chemistry changes the distribution (species/amount/phase) of reactive nitrogen in fresh smoke plumes
- For similar fuel types, NH_x emissions factors are similar to or higher than lab-based estimates; NO_y emission factors are smaller

Emissions of Reactive Nitrogen From Western U.S. Wildfires During Summer 2018

Jakob Lindaas[1], Ilana B. Pollack[1], Lauren A. Garofalo[2], Matson A. Pothier[2], Delphine K. Farmer[2], Sonia M. Kreidenweis[1], Teresa L. Campos[3], Frank Flocke[3], Andrew J. Weinheimer[3], Denise D. Montzka[3], Geoffrey S. Tyndall[3], Brett B. Palm[4], Qiaoyun Peng[4], Joel A. Thornton[4], Wade Permar[5], Catherine Wielgasz[5], Lu Hu[5], Roger D. Ottmar[6], Joseph C. Restaino[7], Andrew T. Hudak[8], I-Ting Ku[1], Yong Zhou[1], Barkley C. Sive[9], Amy Sullivan[1], Jeffrey L. Collett Jr[1], and Emily V. Fischer[1]

[1]Department of Atmospheric Science, Colorado State University, Fort Collins, CO, USA, [2]Department of Chemistry, Colorado State University, Fort Collins, CO, USA, [3]National Center for Atmospheric Research, Boulder, CO, USA, [4]Department of Atmospheric Sciences, University of Washington, Seattle, WA, USA, [5]Department of Chemistry and Biochemistry, University of Montana, Missoula, MT, USA, [6]Pacific Northwest Research Station, USDA Forest Service, Seattle, WA, USA, [7]California Department of Forestry and Fire Protection, Sacramento, CA, USA, [8]Rocky Mountain Research Station, USDA Forest Service, Moscow, ID, USA, [9]Air Resources Division, National Park Service, Denver, CO, USA

Abstract Reactive nitrogen (N_r) within smoke plumes plays important roles in the production of ozone, the formation of secondary aerosols, and deposition of fixed N to ecosystems. The Western Wildfire Experiment for Cloud Chemistry, Aerosol Absorption, and Nitrogen (WE-CAN) field campaign sampled smoke from 23 wildfires throughout the western U.S. during summer 2018 using the NSF/NCAR C-130 research aircraft. We empirically estimate N_r normalized excess mixing ratios and emission factors from fires sampled within 80 min of estimated emission and explore variability in the dominant forms of N_r between these fires. We find that reduced N compounds comprise a majority (39%–80%; median = 66%) of total measured reactive nitrogen (ΣN_r) emissions. The smoke plumes sampled during WE-CAN feature rapid chemical transformations after emission. As a result, within minutes after emission total measured oxidized nitrogen (ΣNO_y) and measured total ΣNH_x ($NH_3 + pNH_4$) are more robustly correlated with modified combustion efficiency (MCE) than NO_x and NH_3 by themselves. The ratio of $\Sigma NH_x/\Sigma NO_y$ displays a negative relationship with MCE, consistent with previous studies. A positive relationship with total measured ΣN_r suggests that both burn conditions and fuel N content/volatilization differences contribute to the observed variability in the distribution of reduced and oxidized N_r. Additionally, we compare our in situ field estimates of N_r EFs to previous lab and field studies. For similar fuel types, we find ΣNH_x EFs are of the same magnitude or larger than lab-based NH_3 EF estimates, and ΣNO_y EFs are smaller than lab NO_x EFs.

Plain Language Summary Smoke from large wildfires in the western U.S. degrades air quality across the whole U.S. Smoke contains a mixture of many different gases and particles, including carbon compounds like carbon dioxide and carbon monoxide, as well as nitrogen compounds such as ammonia and nitrogen oxides. Gases containing nitrogen are important for the production of ozone and the formation of more or larger particles as the smoke moves downwind. During the summer of 2018, we used the National Science Foundation/National Center for Atmospheric Research C130 research aircraft to fly through smoke across the western U.S. and measure many of the most abundant nitrogen compounds. We find that the smoke plumes we sampled emitted more nitrogen in a reduced form than in an oxidized form, and chemical reactions change the form and phase of nitrogen very quickly in the smoke. We compare our field measurements with laboratory measurements with the goal of using them together to improve our forecasts of how and where wildfire smoke will impact air quality.

1. Introduction

Large wildfires are becoming more frequent in the western U.S. (Westerling, 2016) and smoke from large western U.S. wildfires can impact atmospheric composition on a continental scale (Jaffe et al., 2008; Park

et al., 2003, 2007). Smoke is becoming a proportionately larger driver of poor air quality in certain regions in the context of decreasing anthropogenic emissions from many sectors (McClure & Jaffe, 2018; O'Dell et al., 2019), ongoing climate change (Schoennagel et al., 2017; Williams et al., 2019), and fire management practices (Kolden, 2019; Schultz & Moseley, 2019).

Reactive nitrogen (N_r = all N-compounds except N_2O and N_2) within biomass burning smoke contributes to the production of ozone (O_3) (Jaffe & Wigder, 2012), the formation of secondary inorganic (Trentmann et al., 2005) and organic aerosol (Lin et al., 2016), and nitrogen (N) deposition to downwind ecosystems (Chen et al., 2014; Prenni et al., 2014). The form of N_r within smoke ranges from fully reduced (ammonia; NH_3) to highly oxidized (nitric acid; HNO_3). Roughly half of the N emitted by biomass burning is thought to be molecular nitrogen (N_2), an important denitrification process in ecosystems (Kuhlbusch et al., 1991; Lobert et al., 1990). Small molecules such as NH_3, nitric oxide (NO), and isocyanic acid (HNCO) comprise the majority of the remaining N emissions, with smaller contributions from hydrogen cyanide (HCN), nitrous acid (HONO), acetonitrile (CH_3CN), and a wide variety of other N-containing volatile organic compounds (NVOCs, including amine, amide, nitrile, nitro, isocyanate, and N-heterocyclic compounds) (e.g., Coggon et al., 2016).

Fixed N in burning biomass is initially pyrolyzed as a handful of small N-containing compounds: NH_3, HCN, HNCO, and CH_3CN and minor amounts of other NVOCs (Glarborg et al., 2018; Lobert & Warnatz, 1993; Roberts et al., 2020). Immediately following this decomposition of fuel N and subsequent volatilization, and still within the flame, some of these species are quickly oxidized by rapid radical chemistry to form the remainder of the species we consider to be primarily emitted by fires: N_2, NO, NO_2, N_2O, and HONO (Hansson et al., 2004; Ren & Zhao, 2012, 2013a, 2013b; Scharko et al., 2019; Sekimoto et al., 2018). Prior to the FIREX Fire Lab experiments in 2016, laboratory and field studies found strong relationships between the observed forms of N_r emissions and the dominant combustion conditions, with more NO_x and HONO emissions during flaming combustion and more NH_3 and HCN emissions during smoldering combustion (Burling et al., 2010; Goode et al., 1999; McMeeking et al., 2009; Roberts et al., 2010; Yokelson et al., 1996, 1997). Flaming combustion is generally associated with higher burn temperatures and greater oxidation of initially pyrolyzed small N-compounds, with smoldering combustion characterized by lower burn temperatures and lesser oxidation. Fuel moisture and fuel geometry (or arrangement) can affect the combustion characteristics and forms and relative amount of N_r (Chen et al., 2010; McAllister, 2019). Fuel N content has also been shown to be an important determinant of how much N_r is emitted, with higher fuel N generally corresponding to great N_r emissions (Burling et al., 2010; Coggon et al., 2016; Kuhlbusch et al., 1991; Lobert et al., 1990; Stockwell et al., 2014). We note that all N_r emitted by natural convection biomass burning is derived from fuel N, as these fires do not burn hot enough to form thermal NO_x from the reaction of N_2 and O_2 (Roberts et al., 2020). In recent work, Roberts et al. (2020) find pyrolysis temperature, rather than combustion efficiency, to be a more important indicator of emissions variability for HCN, HNCO, and HONO, whereas combustion conditions continued to aptly describe variability in emissions of NO_x and NH_3.

A large wildfire contains a range of burning conditions at any given time. One researcher has described large wildfires as "1,000 small fires all burning differently" (Jack Dibb, personal communication). The mixture of processes in a single wildfire can result in a smoke plume that may have a flaming combustion signature, or a smoldering one (Yokelson et al., 1997), or emissions dominated by pyrolysis and flame oxidation at different temperatures (Roberts et al., 2020; Sekimoto et al., 2018). The combustion temperature is a complex function of fuel moisture, type, geometry and other environmental factors such as turbulence (e.g., McAllister, 2019) and will affect both the form of initially volatilized N as well as the oxidation pathways of N_r in the radical-driven flame chemistry. The most common metric used to describe the integrated burn condition is the modified combustion efficiency (MCE) (e.g., Yokelson et al., 1996), calculated as the ratio of background-corrected carbon dioxide (CO_2) to the sum of background-corrected CO_2 and background-corrected carbon monoxide (CO), shown in Equation 1. MCE values close to one indicate flaming combustion whereas MCE values closer to 0.8 indicate smoldering combustion, and values in between represent a mixture of combustion processes.

$$MCE = \frac{\Delta CO_2}{\Delta CO_2 + \Delta CO} \qquad (1)$$

After emission, N_r compounds in smoke may undergo further oxidation or participate in association reactions and partition into existing aerosol (e.g., Akagi et al., 2012). This chemistry will depend on the presence of oxidants such as OH, O_3, and the nitrate radical (NO_3^-), as well as gas-phase acids and bases and particulate inorganic and organic ions. The products of this N_r evolution will commonly consist of HNO_3, organic nitrates (ONs), nitro-aromatics, acyl peroxy nitrates (APNs), particulate nitrate (pNO_3), and particulate ammonium (pNH_4) (e.g., Alvarado et al., 2010; Liu et al., 2016).

During summer 2018, the Western Wildfires Experiment for Cloud Chemistry, Aerosol Absorption, and Nitrogen (WE-CAN: https://www.eol.ucar.edu/field_projects/we-can) field campaign sampled more than 20 major wildfires throughout the western U.S. The National Science Foundation/National Center for Atmospheric Research (NSF/NCAR) C-130 research aircraft was outfitted with a large suite of trace gas, aerosol, and remote sensing instrumentation and flew 19 research flights from bases in Boise, ID, and Broomfield, CO. The WE-CAN payload included a comprehensive set of N_r trace gas and aerosol measurements optimized for sampling wildfire smoke. Daytime flights included sampling during periods of rapid fire growth, and many smoke plumes were sampled within 1 h of estimated emission. The number and diversity of large fires (>1,000 acres) sampled so close to emission represent one of the most comprehensive sets of in situ wildfire emission data collected to date. Close-by "emissions" transects were typically followed by pseudo-Lagrangian sampling downwind, enabling the aging of fresh smoke to be linked to various physical and chemical evolution processes. In this paper we focus on empirical estimation of N_r emissions from the wildfires sampled by WE-CAN. We explore variability in the dominant forms of N_r between fires, and relate our observations to fuel and combustion differences. We also compare our emission estimates to previous work, in particular lab burns of specific fuels, to investigate the applicability of emission factors (EFs) across diverse fires.

2. Measurements and Methods

2.1. Overview of WE-CAN Sampling Strategy

The WE-CAN project deployed the NCAR/NSF C-130 research aircraft in summer 2018 (22 July–13 September) to sample wildfire smoke during its first day of atmospheric evolution (https://www.eol.ucar.edu/field_projects/we-can). The flight plans and aircraft payload were specifically designed to answer questions related to N_r in wildfire smoke plumes, as well as questions related to absorbing aerosols, cloud activation and other chemical processes in wildfire plumes. Approximately two-thirds of the flight hours (134 total) were focused on sampling emissions and aging of daytime wildfire smoke. The other third of flight hours were devoted to sampling smoke-cloud mixtures. The goal of the emission and aging flight hours was to fly as close to its source as possible given safety and logistical constraints and to systematically characterize the variability in emissions for a wide set of fires burning in different ecosystems under varying environmental conditions. Flight patterns were largely consistent across fires sampled during WE-CAN, with additional sampling added to specific fires. Upon approaching a major wildfire, the aircraft first sampled upwind air to characterize upwind conditions. The aircraft then crossed the smoke plume downwind of the fire as close to the fire as possible. This transect was typically done at a single altitude, but was possible at several altitudes for a subset of fires. From here, the aircraft sampled the smoke through multiple downwind plume transects in order to characterize smoke evolution in a pseudo-lagrangian fashion.

Pseudo-Lagrangian sampling was attempted for 12 fires during WE-CAN, but WE-CAN sampled smoke that could be traced to 23 different wildfires located in eight different western U.S. states. The summer 2018 U.S. wildfire season was very active, the sixth-largest on record in terms of burn area. Within the U.S. 58,083 wildfires burned 8.8 million acres (Hoover & Hanson, 2019). Thus, the aircraft was able to opportunistically sample many fresh smoke plumes en route to or returning from the target wildfires. For the purposes of this emissions-focused analysis, we define 26 unique sampling periods within 80 min estimated physical age of emission. Extending the threshold to 100 min only adds a single sampling period, and lowering it to 60 min reduces the number of sampling periods by 25%. Our main conclusions do not change in either case. These "emissions transects" correspond to 16 individual fires, of which several were sampled over different days or multiple discrete times within 1 day (defined as transects greater than 30 min apart). The WE-CAN flights spanned the period of the day with the greatest wildfire activity and the easiest aircraft access. During the majority of the campaign, when the aircraft was based in Boise, ID, the flights typically took off between
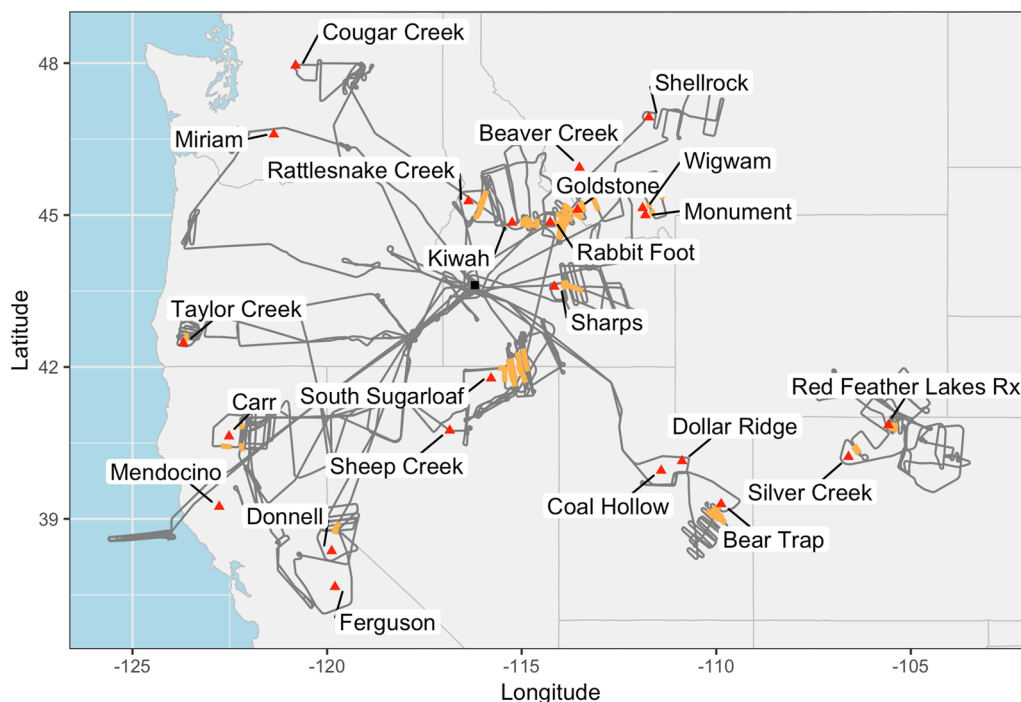
Figure 1. Flight tracks during WE-CAN (gray) with fires sampled (red triangles and labels) and plume segments used in this analysis highlighted in orange. The black square denotes our base of operations in Boise, ID.

12:00 and 14:00 Local Time (Mountain Time = UTC - 6 h), and landed between 19:00 and 21:00 Local Time. WE-CAN sampled a mixture of fire sizes, ignition types, and fuel types. The final burn area of fires sampled during WE-CAN ranged from less than 5,000 acres (e.g., Wigwam Fire) to more than 450,000 acres (Mendocino Complex Fire). Each fire was associated with the Fuel Characteristic Classification System (FCCS) fuelbeds that burned during the specific time the NSF/NCAR C-130 aircraft was sampling the smoke (Ottmar et al., 2007). The fires sampled during WE-CAN (red triangles), along with the flight tracks (gray lines), are shown in Figure 1. The orange segments signify the portion of the dataset used in the analysis presented here.

2.2. Measurement Details

WE-CAN measurements include a large suite of gas-phase and particle-phase reactive N species. Instruments in the payload responsible for measured N_r species and the key carbon species used in the analysis include: the NCAR 2-channel and single-channel chemiluminescence instruments measuring NO, NO_2, and O_3; the Colorado State University (CSU) QC-TILDAS measured gas-phase NH_3; the University of Washington (UW) I-CIMS measuring HCN, HNCO, HNO_3, HONO, and gas-phase organic nitrates; the NCAR PAN-CIMS measuring PAN and PPN; the University of Montana (UM) PTR-ToF-MS measuring acetonitrile (CH_3CN) and a selection of NVOCs (amines: ethenamine, propene amine, trimethylamine, butene amine; amides: formamide and acetamide; nitriles: propane nitrile, hydroxy acetonitrile, cyanoallene isomers, pentanenitriles, 4-methylpentanenitrile, benzonitrile, furancarbonitriles; nitro species: nitromethane, nitropropanes, nitroethane, nitroethene, nitrotoluene; and N-heterocyclics: pyrrole, dihydropyrrole, pyridine, methyl pyrrole isomers, ethylnylpyrrol, methyl pyridines, vinylpyridine, dihydroxy pyridine, nitrofuran); the CSU AMS measuring pNH$_4$ and pNO$_3$; the NCAR QC-TILDAS measuring CO and nitrous oxide (N_2O); the NCAR Picarro measuring CO_2, CO, and CH_4; the CSU PILS measuring inorganic NH_4 and NO_3 ions; and the NCAR AWAS which was used to collect whole air samples from which a suite of VOCs were measured at CSU, including measurements of seven alkyl nitrates (methyl-to pentyl-). To our knowledge, there are no published examples of in situ wildfire plume observations where most of the key species relevant to determining the ratio between oxidized and reduced N, or the rapid conversion of NO_x to its oxidation products

(e.g., PANs, organic nitrates, HNO_3) have been simultaneously quantified. However, the WE-CAN payload did not include a measurement of total oxidized N (NO_y) or total N_r, or speciated gas-phase and particulate organic nitrates. Roberts et al. (2020) used a similar set of gas-phase measurements in the lab and compared the sum N_r (without particulate N) to a measurement of total N_r. They estimated that the sum of individual gas-phase N_r compounds captured between 75% and 95% of the total N_r emitted, with the remainder expected to be low and semi-volatile N compounds. In lieu of a total NO_y or N_r measurement, in our analysis we will use the sum of measured species, ΣNO_y ($= NO_x + pNO_3 + PANs + HNO_3 + HONO + ONs$) and ΣN_r ($=$ sum of all measured N). In the following sections we describe the instruments listed above.

2.2.1. NCAR NO_x/O_3

NO and NO_2 were measured with the NCAR 2-channel chemiluminescence instrument; the NCAR single-channel chemiluminescence instrument for measuring O_3 was integrated with this system. The instruments shared an inlet, pumping system, data acquisition system, and power supplies. NO is measured via its chemiluminescent reaction with a flow of reagent O_3, generated on board (Ridley & Grahek, 1990). Photons from excited NO_2 are counted with a dry-ice-cooled photomultiplier tube to provide the primary signal. NO_2 is measured in a separate sample flow as an increase in NO following photolysis of NO_2 by "400 nm" light-emitting diodes (LEDs, model LZP-00UA00, bin code U5, with actual peak wavelengths of 390–395 nm and a spectral width of ~10 nm). Interference from HONO on the NO_2 measurement is expected to be small given the factor of 40–150 larger NO_2 cross sections in the LED wavelength range. O_3 is measured similarly via the reaction of ambient O_3 with a flow of reagent NO from an on-board gas cylinder (Ridley et al., 1992). The NO and NO_2 channels are periodically calibrated in flight using two flows from a compressed gas calibration standard of NO in N_2, one of which has O_3 added in order to convert NO to NO_2 for the calibration of the NO_2 conversion efficiency by the LEDs. The O_3 channel was calibrated periodically on nonflight days using a Thermo Scientific Primary Standard, Model TEI 49i-PS, factory calibrated in April 2018. Data are reported at 1 Hz, though the time response of the NO_x channels is somewhat slower than this. At mixing ratios >1 ppbv the uncertainties are 6% for NO, 12% for NO_2, and 5% for O_3 and the upper bound on mixing ratio dependant precision is 100 pptv for NO, 140 pptv for NO_2, and 0.2 ppbv for O_3.

2.2.2. CSU NH_3

NH_3 was measured using a compact, single-channel, closed-path quantum-cascade tunable infrared laser direct absorption spectrometer (QC-TILDAS). In order to improve accuracy and time response, the commercially available instrument (from Aerodyne Research Inc.) was augmented with (1) a heated PFA aircraft inlet, (2) an inertial inlet that separates particles with aerodynamic diameters greater than 300 nm from the sample stream, (3) a continuous flow of passivant (1H, 1H-perfluorooctylamine: a stronger base than NH_3) which coats inlet surfaces and improves NH_3 transmission, and (4) a custom-designed, vibrationally isolated plate. This system is described in detail by Pollack et al. (2019) and descriptions of the commercially available QC-TILDAS have been previously published (McManus et al, 1995, 2007, 2010; Zahniser et al., 1995). During WE-CAN the NH_3 QC-TILDAS collected NH_3 mixing ratio measurements at 10 Hz and were averaged to 1 Hz, with a 3σ detection limit of ± 200 pptv, an uncertainty of $\pm 12\%$ of the measured mixing ratio plus the detection limit, and a response time of ~1 s corresponding to 90% signal recovery.

2.2.3. UW I-CIMS

Gas-phase HCN, HNCO, HNO_3, HONO, and organic N-containing compounds were sampled by the UW high-resolution chemical ionization time-of-flight mass spectrometer using iodide-adduct ionization (I^--CIMS; Lee et al., 2014, 2018). Ambient air was sampled at 20 lpm through a straight ~50 cm length of 0.75 in OD PTFE Teflon tubing. The air was then subsampled at 2 slpm into a custom ion-molecule reaction (IMR) inlet designed to minimize the influence of walls on the measurements while characterizing the remaining wall effects, as described in Palm et al. (2019). The mass spectrometer simultaneously measured hundreds of molecular formulas, including inorganic and oxidized organic molecules, at 2 Hz time resolution and with a mass resolving power of ~5,000. Water vapor was continuously added to the IMR in order to maintain relatively constant water vapor concentrations and minimize the effects of water vapor dependence on the ionization process. The IMR background signal was measured for 6 s each 1 min by overflowing the IMR with clean N_2 gas. The background signal from the inlet tubing was also measured for 15 s every 15 min. HCN, HNCO, HNO_3, and HONO were each calibrated in the laboratory before and/

or after WE-CAN deployment. Calibration factors and details specific to the WE-CAN deployment can be found in Peng et al. (2020), but in general are similar to those reported previously (Lee et al., 2014, 2018). For these species, accuracy is estimated to be 30% and detection limits, propagated from the standard deviation of 1 s data, are 112 pptv for HCN, 70.4 pptv for HNCO, 20.5 pptv for HNO_3 and 13.5 pptv for HONO. Gas-phase multifunctional organic nitrates (ONs) are also detected by the I-CIMS, with ONs defined as any species containing N, two or more carbon atoms, and three or more oxygen atoms. Individual ONs and isomers cannot be separated or directly calibrated. While the I-CIMS does not provide specific information on molecular structure or functional groups, the nature of iodide-adduct ionization means the detected compounds are most likely multifunctional organic nitrates, peroxy nitrates, and/or peroxyacyl nitrates (Lee et al., 2016). Multifunctional oxidized amines are also theoretically possible but are not expected. Thus for simplicity, we refer to this group of measured compounds as gas phase ONs. Therefore, an estimate of ΣONs is made by assigning a calibration factor of five normalized counts per second (ncps) per pptv of analyte for all organic nitrates detected and summing over all ONs. This calibration factor is an estimate of the average sensitivity for this group of compounds, and is based on the range of sensitivities of calibrated gases during WE-CAN. This ΣONs calculation has large uncertainties, estimated here as a factor of two on the absolute mixing ratio (200% error). Gas-phase nitrophenolic species are not included in this sum ONs, but are a small fraction (<1%) of total gas-phase ON mass. Most nitrophenolic compounds are expected to be in the particle phase and would therefore be detected by the AMS. To avoid double-counting PAN and PPN and since the PAN-CIMS is more sensitive and precise, we removed their corresponding molecular formulas from the I-CIMS ΣONs calculation.

2.2.4. NCAR PAN-CIMS

PAN and PPN were measured with a thermal dissociation chemical ionization mass spectrometer (CIMS) (Slusher et al., 2004; Zheng et al., 2011). PANs in ambient air are decomposed in the instrument inlet at 150°C into NO_2 and the parent peroxy acyl radicals. The latter react with Iodine ions produced from CF_3I in a static ionizer cartridge in the flow tube controlled to a pressure of 20 torr. The produced acylate ions are then detected in a quadrupole mass spectrometer. Calibration is performed continuously by adding a known amount of isotopically labeled C^{13}- PAN to the aircraft inlet. Accuracy is 12% or 25 pptv (whichever is greater) for PAN and PPN and precision is 20 pptv on average across the flights.

2.2.5. UM PTR-ToF-MS

VOC measurements were made using a proton-transfer-reaction time-of-flight mass spectrometer (PTR-ToF-MS 4000, Ionicon Analytik). In brief, ambient air is continuously pumped through the PTR-ToF-MS drift-tube, where VOCs with a proton affinity higher than that of water (>165.2 kcal/mol) are ionized via proton-transfer reaction with H_3O^+ ions, then subsequently separated and detected by a time-of-flight mass spectrometer (with a mass resolving power up to 4,000). During WE-CAN, PTR-ToF-MS measured ion m/z from 15–400 at 2 or 5 Hz frequency. Ambient air was drawn to the instrument at 10–15 lpm via ∼3 m of 1/4" O.D. PFA tubing maintained at ∼55°C, and then subsampled by the instrument though ∼100 cm of 1/16" O.D PEEK tubing maintained at 60°C. The residence time from outside of the aircraft to the drift-tube is less than 2 s. Instrument background was checked approximately every hour during a flight by measuring VOC-free air generated from a heated catalytic converter (375°C, platinum bead, 1 % wt. Pt, Sigma Aldrich). Calibrations were typically performed 3 times per flight by the dynamic dilution of certified gas standard mixtures containing 25 distinct VOCs (Apel-Riemer Environmental Inc.,). For ions not directly calibrated by the gas standard, sensitivities were estimated using the method described by Sekimoto et al. (2017). Measurement uncertainties for the 25 directly calibrated VOCs are ∼15%, and for the rest are estimated to be better than 50%. Detection limits are species specific and generally range 50–250 pptv for directly calibrated VOCs (Yuan et al., 2017).

2.2.6. CSU AMS

Chemically-resolved submicron nonrefractory aerosol mass was measured using a high-resolution time-of-flight aerosol mass spectrometer (HR-TOF-AMS; Aerodyne, Inc.) (DeCarlo et al., 2006) equipped with a pressure controlled inlet (Bahreini et al., 2008). Operation of this instrument and data processing during WE-CAN is described in Garofalo et al. (2019). Briefly, in the HR-TOF-AMS, particles are focused through an aerodynamic lens to a tungsten vapourizer (standard vapourizer) at 600°C; the resulting gases are ionized

by 70 eV electron ionization, and subsequently extracted and analyzed by time-of-flight mass spectrometry. During WE-CAN, the HR-TOF-AMS was operated in standard mass spectrometry mode with 5 s time resolution (2.5 s open and 2.5 s closed) in V-mode (m/Δm ∼2,100). Accuracy (2σ) for the HR-AMS is estimated to be 35% for inorganic species (Bahreini et al., 2009). At low concentrations, precision is the same as the detection limit - better than 0.1 ug sm^{-3} for pNO$_3$ and pNH$_4$ at 5s time resolution. At high concentrations, precision is 0.5%–3% of pNO$_3$ and pNH$_4$ mass. We note that due to the nature of electron ionization, organic nitrates, if present, will fragment to NO$_x^+$ ions in the AMS, and thus may contribute to reported pNO$_3$ (Farmer et al., 2010). Determination of the relative contribution of organic nitrates to the pNO$_3$ signal for this dataset is currently underway. We use the notation pNO$_3$ here to indicate that both inorganic and organic N-containing species may contribute to this signal. Similarly, reduced N-containing organics such as amines and amides may contribute to the observed pNH$_4$ signal and the reported pNH$_4$ should be considered an upper bound for sub-micron particulate ammonium (NH$_4^+$).

2.2.7. NCAR CO/N$_2$O/CO$_2$/CH$_4$

CO and N$_2$O were measured with a commercial Mini-TILDAS tunable diode laser infrared absorption spectrometer (Aerodyne Research) (Lebegue et al., 2016). To optimize measurement accuracy, the spectrometer optical bench was continuously purged with synthetic zero grade air from which CO had been scrubbed to contain less than 1 ppbv. N$_2$O was quantified in the purge gas and typically found to contain less than 0.3 ppbv. This constant N$_2$O purge gas concentration at cabin pressure was included in spectral fit calculations to better reproduce spectral background. The WE-CAN data set has a precision of 0.1 ppbv with a 2s temporal resolution and an accuracy of ±0.6 ppbv for CO and ±1 ppbv for N$_2$O. A Picarro G-2401-m analyzer was used for the measurement of CO$_2$ and CH$_4$, which also provided an additional, but lower precision, measurement of CO. Stated 1σ precision for the Picarro is 30, 20, and 2 ppbv for CO, CO$_2$ and CH$_4$, respectively. Accuracy for the Picarro CO$_2$ measurements is 0.05 ppmv. Calibration was done by overflowing the inlet with a known mixture of the measured gases in ultrazero air at regular intervals during flight.

2.2.8. CSU Particle-Into-Liquid Sampler (PILS)

Two minute integrated inorganic particulate NO$_3^-$ and NH$_4^+$ were determined using a Particle-into-Liquid Sampler (PILS) with fraction collector system. The operation of the PILS system and off-line analysis of the liquid samples by ion chromatography were conducted similar to during the WINTER (Wintertime Investigation of Transport, Emissions, and Reactivity) Campaign (Sullivan et al., 2019). Accuracy is estimated to be 10% and precision is 0.4 ug m^{-3}.

2.2.9. Whole Air Samples

During WE-CAN the NCAR community requestable Advanced Whole Air Sampler (AWAS) system (Andrews et al., 2016) (www.eol.ucar.edu/instruments/advanced-whole-air-sampler) was operated by CSU. The AWAS collects canister samples for off-line analysis of VOCs. For WE-CAN up to 46 canister samples could be collected per flight triggered by an on-board operator. Typically a background sample was collected upwind of the fire and 1–3 samples per plume crossing. This included (as possible) a sample when transitioning into the smoke, at the peak of the smoke, and when exiting the smoke. Following each flight the canisters were shipped to CSU to be analyzed for a total of 61 individual VOCs (C$_1$–C$_{10}$ NMHCs, C$_1$–C$_5$ alkyl nitrates and oxygenated VOCs) using a five-channel GC (gas chromatograph) system equipped with three flame ionization detectors (FIDs), one electron capture detector (ECD) and one mass spectrometer. More details on the instrument and analysis methods can be found in Russo et al. (2010), Zhou et al. (2010), and Benedict et al. (2019). The measurement precision is based on repeated analysis of two calibrated whole air standards that ranged from 1% to 8% for the NMHCS (nonmethane hydrocarbons) and 3% to 5% for the alkyl nitrates (Russo et al., 2010). The accuracy of the alkyl nitrates is 10% to 20% and the detection limit is 0.01 pptv.

2.3. Fuels Classification

Wildland fuels that burned during each of the WE-CAN flights were characterized and summarized using the Fuel Characteristic Classification System (FCCS). FCCS defines a fuel bed as the inherent physical characteristics of aboveground biomass and classifies wildland fuel characteristics at 30-m resolution to predict

surface fire behavior and available fuel for consumption and emissions estimation. We used FCCS maps generated from LANDFIRE 2014 (Rollins, 2009) in combination with incident specific perimeter mapping to estimate the fuels burned during each research flight. Specifically, we acquired daily infrared fire perimeters for each wildfire bracketing the times of each research flight. The primary sources for incident specific spatial heat perimeter data included the National Interagency Fire Center (NIFC) FTP Server (https://ftp.nifc.gov/public/incident_specific_data/) and the Geospatial Multi-Agency Coordination (GeoMAC) funded by the Geosciences and Environmental Change Center (https://rmgsc.cr.usgs.gov/outgoing/GeoMAC/). We assigned a rating system for data quality that relates the match quality between the timing of the heat perimeter data and the times of the research flights. Once we vetted the daily perimeter data, we were able to use ArcGIS to summarize the wildland fuels that burned during each research flight. Fuels were summarized in descending order from most to least abundant wildland vegetation types. The X and Y field centroid of the burn area was identified for each flight using the Geometry tool in ArcGIS, and used as the fire location coordinates for further analysis.

LANDFIRE 2014 incorporates landscape change and disturbances, such as wildland fire, fuel and vegetation treatments, insects and disease, storm damage, and invasive plants that occurred in 2013 and 2014. As such, this layer does not represent elements of landscape change from 2014 to 2018. This is one of the larger potential sources of error in this analysis. We also focused exclusively on mapping the best available heat perimeters to bracket each research flight. This is a good metric for measuring new actively burning areas, but does little to estimate contributions from smoldering material from the day(s) preceding the research flights.

2.4. Plume Criteria

We define a plume transect as an individual leg of the flight that transects the smoke plume from background air through the plume and out again into background air. These transects were as close to perpendicular to the plume transport direction as pilots and navigational constraints would allow. Start and end times for plume transects are chosen visually using the correlated rapid increase and decrease of tracers such as CO, black carbon, HCN, and NH_3. Plume transects used in this analysis range from 0.66 to 8.4 min long (median of 2.6 min), much longer than the sampling rate of most in situ instruments.

To estimate the physical age of the smoke sampled, we use the distance from the center of the plume transect to a centroid of the active burn area and divide it by the average wind speed across the transect. We recognize that uncertainties in the active burn location, friction, and entrainment, along with variable winds along the plume trajectory, may cause this estimate to deviate from the true age. These factors could lead to differences in physical age across individual plume transects. However, this method is intended to capture the average behavior of the plume once it is entrained in the mean atmospheric flow.

For this analysis, we use plume transects with estimated physical ages < 80 min as "emission transects." The youngest smoke sampled was ∼ 20 min old, while navigation and safety constraints limited the ability of the NSF/NCAR C-130 to fly within an hour of emission on several large fires. Normalized excess mixing ratios (NEMRs) and emission factors (EFs) calculated from plume transects sampled within a period of 30 min are averaged and assumed to represent one emissions pass for that fire. If another set of plume transects on the same fire was sampled > 30 min later in flight time, then they are averaged and considered a separate emissions pass. Plume transects with ages > 80 min will be analyzed and discussed in forthcoming papers concerning different aspects of N_r evolution within smoke plumes.

2.5. Normalized Excess Mixing Ratio (NEMR) Calculations

In comparing abundances of a species of interest between different smoke plumes, it is useful to normalize the measurements by dividing by the abundances of a conserved tracer. This conserved tracer accounts for dilution, and is typically CO, or HCN. This ratio is called the normalized excess mixing ratio (NEMR) of species X. Problems arise in the interpretation of NEMRs when the composition of background air is changing (Yokelson et al., 2013a). There can be large (i.e., orders of magnitude) variability in NEMRs for a given fire even in a controlled setting (Gilman et al., 2015). Two methods are commonly used to calculate NEMRs

in wildfire smoke plumes: the integration method, and the slope method (Yokelson et al., 2013b). Both approaches assume that different parts of the plume segment are not coming from different parts of the fire, which might be burning at different stages. Briefly, the integration method subtracts the background of X from the time series of X, and the background of CO from the timeseries of CO, then divides the sum of ΔX by the sum of ΔCO to calculate the NEMR. One strength of this method is that it integrates across all the mass in a given plume transect, while requiring the identification or estimation of a background for each species. The slope method calculates the NEMR by finding the slope of an orthogonal least squares fit to the relationship between CO and species X. This approach assumes the data are perfectly time-aligned, and does not need a separate background estimate, but it is sensitive to the chemistry in the most dense parts of the plume driving the overall NEMR. The intercept of the fit can be used to estimate a background if desired.

In this analysis, we use the integration method for calculating nearly all NEMRs, in order to enable a more robust total mass conversion of NEMR to EFs. The only exception is the NEMR of CO_2, where the slope method allows for a more robust calculation of MCE from the CO_2/CO ratio. To estimate the background for each perpendicular plume transect, we average 15 s of measurements before and after entering and exiting the plume, respectively. Most of the observations used in our analysis were collected at 1-Hz or higher. In these cases, only data points with valid measurements of both species X and CO are used in calculating ΔX and ΔCO. AMS data was reported on a 5-s timebase, and these data are merged with the 1 s data, and converted into mixing ratio equivalent from standard mass concentration units (conversion described in the supplement). Amendments to these methods were made for AWAS data, measuring a snapshot of several seconds at discrete intervals, and for PILS data, measuring continuously on a 2 min average timebase. These amendments are described in full detail in the supplemental information. For all measurements, if data are missing during a specific plume transect then the NEMR for that species on that transect is not included in our analysis. Table 1 lists which NEMRs are missing for each fire (Figures S2 and S3 show this visually), and in Figure 2 we replace these missing NEMR values with the average NEMR across all emissions transects. This enables a more representative comparison of ΣN_r measured and its distribution. No substitution of average NEMRs for missing values are presented elsewhere in the paper.

2.6. Emission Factor (EF) Calculations

In the lab, it is possible to measure the mass of a species of interest emitted per mass of fuel burned. This quantity is called an emission factor (EF) in units of grams X per kilogram fuel or biomass, and is widely used as an input to estimate emissions in emission inventories. To calculate an EF based on our field measurements, we follow the total carbon mass balance method outlined in Liu et al. (2017). This method assumes that all of the volatilized carbon is detected, following Yokelson et al. (1999) and Liu et al. (2016). Equation 2 summarizes the calculation:

$$EF_X = \frac{\Delta X}{\Delta CO} \times \frac{1}{\sum \frac{n\Delta C}{\Delta CO}} \times \frac{MW_X}{MW_C} \times \%C \text{ in fuel} \times 1000 \text{ g/kg} \tag{2}$$

Here, the NEMR of species X is divided by the sum of NEMR of all carbon species measured (with n equaling the number of carbon atoms in each species) and then converted to mass by multiplying by the ratio of the molecular weight of X and the atomic weight of C, the estimated percentage of carbon in biomass, and the unit conversion from kilograms (kg) to grams. In this analysis we assume the mass of carbon in 1 kg biomass is 0.457 kg, or 45.7% based on the analysis of Russo et al., 2010, Santí n et al., 2015, Yokelson et al., 2013. We also assume total VOCs and black carbon make up < 3% of total carbon in smoke (following Yokelson et al., 1999), simplifying the sum of carbon NEMRs to Equation 3:

$$\sum \frac{n\Delta C}{\Delta CO} = \frac{1 * \Delta CO_2}{\Delta CO} + \frac{1 * \Delta CO}{\Delta CO} + \frac{1 * \Delta CH_4}{\Delta CO} \tag{3}$$

This assumption will mean that presented values could be an overestimate of the true EF by a few percent. This is small compared to the observed variability and uncertainty associated with our EF estimates.

Table 1
Basic Information for Smoke Plumes Used in This analysis

Fire ID	Fire location	Fuels present	Number of transects	Mean age (min)	Missing/excluded measurements
Bear Trap Fire RF09 a	39.29312, −109.87434	pinyon, douglas fir, engelmann spruce, bigtooth maple, white fir, ponderosa pine, gambel oak, juniper	3	54	-
Bear Trap Fire RF09 b	39.29312, −109.87434	pinyon, douglas fir, engelmann spruce, bigtooth maple, white fir, ponderosa pine, gambel oak, juniper	1	62	N_2O
Beaver Creek Fire RF11	45.93701, −113.51476	lodgepole pine, whitebark pine, subalpine fir, engelmann spruce	1	58	-
Carr Fire RF02 a	40.63087, −122.5196	jeffrey pine, ponderosa pine, live oak, blue oak, black oak, douglas fir, wheatgrass, cheatgrass, chamize, knobcone pine, scrub oak, white fir, red fir	2	67	PAN, PPN
Carr Fire RF02 b	40.63087, −122.5196	jeffrey pine, ponderosa pine, live oak, blue oak, black oak, douglas fir, wheatgrass, cheatgrass, chamize, knobcone pine, scrub oak, white fir, red fir	1	62	N_2O, PAN, PPN, PILS NH_4, PILS NO_3, HONO
Donnell Fire RF07	38.36457, −119.88161	red fir, douglas fir, ponderosa pine, jeffrey pine, sugar pine, tanoak	2	79	-
Goldstone Fire RF10	45.10841, −113.56241	lodgepole pine, douglas fir, ponderosa pine	2	38	N_2O
Kiwah Fire RF06 a	44.85122, −115.24404	douglas fir, ponderosa pine, lodgepole pine, willow, sagebrush, sedge, grassland	4	56	-
Kiwah Fire RF06 b	44.85122, −115.24404	douglas fir, ponderosa pine, lodgepole pine, willow, sagebrush, sedge, grassland	1	70	N_2O, PILS NH_4
Monument Fire RF10	44.99973, −111.82156	whitebark pine, subalpine fir, douglas fir, ponderosa pine, engelmann spruce	1	30	N_2O, PILS NH_4
Rabbit Foot Fire RF06	44.85753, −114.26653	ponderosa pine, subalpine fir, whitebark pine, douglas fir	3	41	-
Rabbit Foot Fire RF10	44.85753, −114.26653	urban, whitebark pine, subalpine fir, douglas fir, ponderosa pine	3	53	N_2O
Rabbit Foot Fire RF11	44.85753, −114.26653	douglas fir, ponderosa pine, sagebrush, whitebark pine, subalpine fir, quaking aspen, engelmann spruce	4	63	N_2O
Rattlesnake Creek Fire RF01	45.27518, −116.36568	ponderosa pine, wheatgrass, douglas fir	2	71	N_2O, PAN, PPN, NO, NO_2
Red Feather Lakes Rx Fire RF18 a	40.852, −105.576	ponderosa pine, douglas fir, ceanothus, gambel oak	4	31	N_2O, HCN, HNCO, HNO_3, HONO, ΣONs, PILS NH_4, PILS NO_3
Red Feather Lakes Rx Fire RF18 b	40.852, −105.576	ponderosa pine, douglas fir, ceanothus, gambel oak	3	39	N_2O, HCN, HNCO, HNO_3, HONO, ΣONs, PILS NH_4, PILS NO_3
Sharps Fire RF04 a	43.58734, −114.1623	sagebrush	2	54	-
Sharps Fire RF04 b	43.58734, −114.1623	sagebrush	1	79	-
Silver Creek Fire RF19	40.22616, −106.60233	quaking aspen, engelmann spruce, subalpine fir, lodgepole pine, whitebark pine	2	26	N_2O, HCN, HNCO, HNO_3, HONO, ΣONs, PILS NH_4, PILS NO_3
South Sugarloaf Fire RF15 a	41.77587, −115.78555	sagebrush, quaking aspen, subalpine fir, douglas fir, engelmann spruce, lodgepole pine	2	48	CH_3CN, $\Sigma NVOCs$
South Sugarloaf Fire RF15 b	41.77587, −115.78555	sagebrush, quaking aspen, subalpine fir, douglas fir, engelmann spruce, lodgepole pine	2	67	CH_3CN, $\Sigma NVOCs$
South Sugarloaf Fire RF15 c	41.77587, −115.78555	sagebrush, quaking aspen, subalpine fir, douglas fir, engelmann spruce, lodgepole pine	1	73	CH_3CN, $\Sigma NVOCs$
South Sugarloaf Fire RF15 days	41.77587, −115.78555	sagebrush, quaking aspen, subalpine fir, douglas fir, engelmann spruce, lodgepole pine	4	48	CH_3CN, $\Sigma NVOCs$

Table 1
Continued

Fire ID	Fire location	Fuels present	Number of transects	Mean age (min)	Missing/excluded measurements
Taylor Creek Fire RF03	42.46705, −123.68992	douglas fir, jeffrey pine, ponderosa pine, tanoak, black oak, madrone	4	29	-
Wigwam Fire RF10	45.13977, −111.89273	douglas fir, ponderosa pine, lodgepole pine, subalpine fir, whitebark pine, engelmann spruce	2	38	N_2O, PILS NH_4, PILS NO_3

Note. Missing measurements indicate that an instrument was not operating or was not sampling ambient air during a given smoke pass (e.g., during zeroes or calibrations). RF17–RF19 were educational flights with a reduced instrument payload. Excluded measurements are specific to N_2O and refer to when N_2O NEMRs are not reported due to nonphysical negative enhancements. Lastly, sampling periods with available PILS NO_3 measurements but missing PILS NH_4 measurements reflect periods when measurements of PILS NH_4 were below the detection limit.

2.7. Uncertainties

Uncertainty in NEMRs and EFs is propagated from the reported precision and accuracy of each measurement, summed in quadrature. In cases where multiple NEMRs or EFs are averaged the uncertainty reported is the root square sum of the standard deviation and the propagated uncertainties from each individual estimate.

3. Results and Discussion

3.1. ΣN_r Partitioning

Figure 2a shows that the total measured excess mixing ratio of ΣN_r relative to CO varies between 0.033 and 0.099 ppbv/ppbv, or 3.3%–9.9% of CO in emission transects. Warm colors here indicate measured reduced N_r species, whereas the cooler green and blue colors denote oxidized N_r species. The total ΣN_r NEMR varies by a factor of three between fires, much larger than the variability within emission transects of the same fire (separated by at least 30 min). However, it's important to recognize the total observed ΣN_r is a lower bound estimate, since there are minor missing measurements of N_r species expected to be present in smoke. The star above specific emission transects indicates that a NEMR for at least one species was missing and was filled in using the average of the NEMR for that species from the other emission transects. N_r species with the largest emission transect enhancements include gas-phase NH_3, NO_2, and HONO, as well as pNH_4 and pNO_3. NEMRs for seven alkyl nitrates from methyl-up to pentyl-nitrate were also calculated from the AWAS data (method described in supplement), but together contribute less than 1% of the total measured ΣN_r, thus are not shown in Figure 2. Figure S1 in the supplement shows the same composite ΣN_r replacing the AMS measurements with ions as measured by the PILS. PILS measurements of NO_3^- and NH_4^+ ions are generally smaller than AMS measurements of total pNO_3 and pNH_4, and offer an estimate of the inorganic aerosol N contribution. Work is ongoing to elucidate the differences between the AMS and PILS measurements and to partition the AMS pNO_3 and pNH_4 into inorganic and organic components. Regardless, the overall conclusions from Figure 2 continue to hold when replacing the AMS species NEMRs with PILS ion NEMRs, except that NO_3^- and NH_4^+ make substantially smaller contributions to ΣN_r. Figures S2 and S3 plot each N_r species' NEMRs per fire in separate panels, showing where data are missing and what variability exists in each species' NEMRs.

Figure 2b displays the relative proportions of the measured ΣN_r NEMRs for the same emission transects. Sums greater than one are possible in the case of negative NEMRs for HNO_3 or N_2O, discussed below, and a star above a given bar again indicates that a missing NEMR was filled in with the average NEMR prior to calculating the percentage contribution. We find that reduced N_r species generally make up more than half of the of total observed ΣN_r (39%–80%; median = 66%), with NH_3 making the largest contribution followed by pNH_4, HCN, and HNCO, and CH_3CN. Oxidized N_r species are dominated by NO_2, HONO, pNO_3, and ΣONs, with variability in the relative contributions of each. On average smaller NO_y contributors to the total observed ΣN_r include NO, PAN, and PPN. NO_x does not make up the majority of measured ΣNO_y in most of these emission transects. The sum of N organic compounds measured by the PTR-ToF-MS ($\Sigma NVOCs$), not
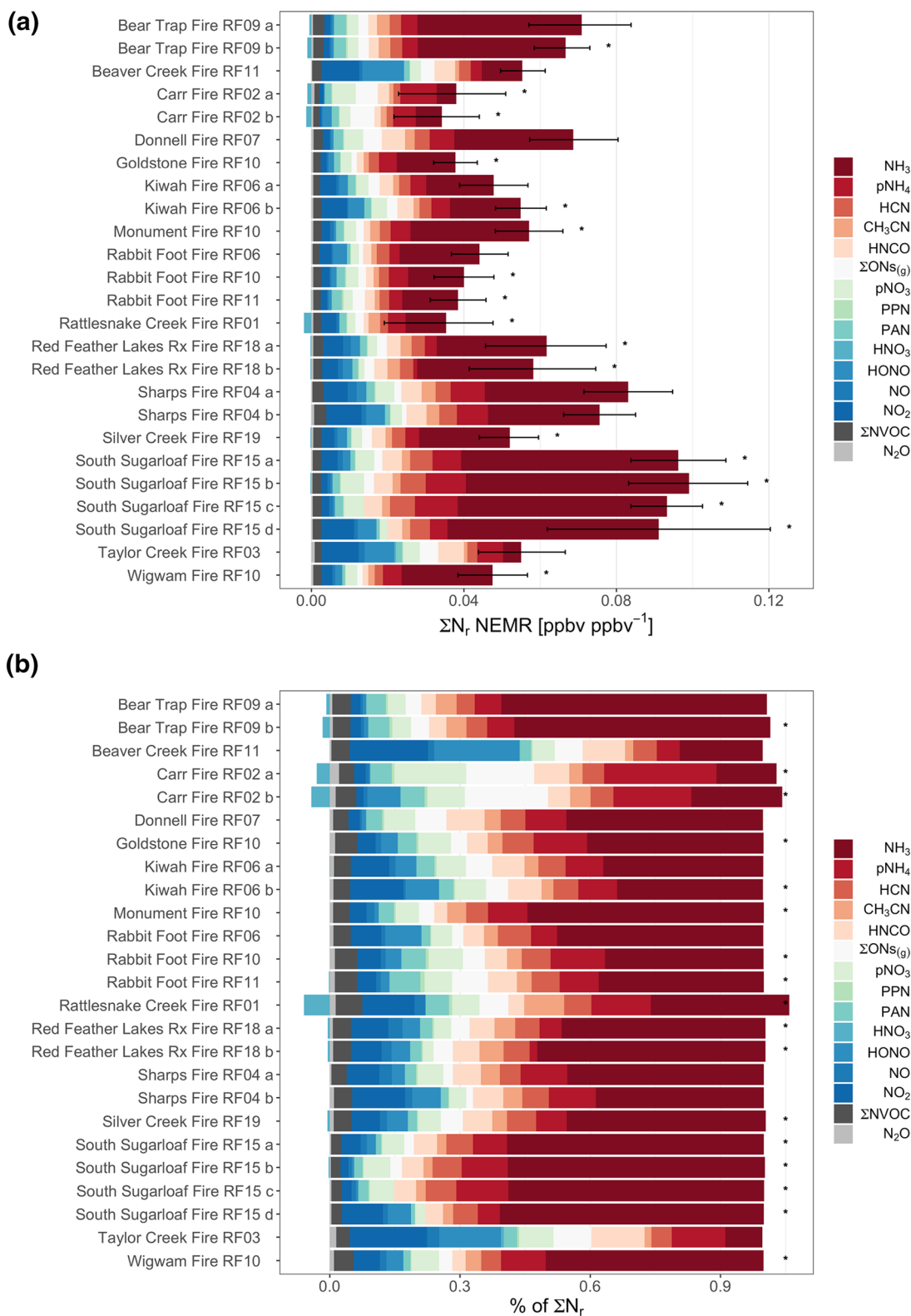
Figure 2. (a) Normalized excess mixing ratios (NEMRs) of measured N_r species for emission transects of WE-CAN fires. Asterisks indicate one or more NEMR estimates are missing and were filled using the mean NEMR for that species across the rest of the emission transects. (b) Fractional contribution to total measured reactive nitrogen (ΣN_r) measured in young smoke plumes during WE-CAN. Sums greater than one during some emission transects reflect small negative NEMRs for HNO_3 as described in the text. pNH_4 and pNO_3 data are from the AMS.

including CH_3CN, account for between 2% and 6% of ΣN_r, and, given the uncertainties in the NVOC measurements and number of other likely unquantified NVOCs, this is likely a lower bound for the contribution of all NVOCs to total N_r. The estimated physical age of these transects ranges from 20–80 min, and given the large abundances of PAN even in the freshest plumes we find evidence of previous conversion of NO_x to other NO_y species. This rapid chemical evolution appears to occur even in the densest smoke plumes. Another key finding of WE-CAN is that there can be significant emissions of HONO relative to NO_x. The impact of this is discussed in Peng et al. (2020) and this finding is consistent with laboratory experiments (Selimovic et al., 2018). Here, we simply note this in the context of all the N_r emission ratios we were able to calculate.

Table S1 (csv in the supplement) provides a summary of NEMRs and EFs for all measured N_r species by individual fire plume transect, along with the calculated MCE. Estimated physical age, and location and fuel type information are shown in Table 1 as well as provided in the supplement. As noted above, small negative NEMRs are estimated for HNO_3 for some emission transects. This is due to lower mixing ratios measured inside the plume as compared to the background values outside the plume. In the case of HNO_3, this could be due to rapid reaction of background and possible plume produced HNO_3 with fire-emitted NH_3 and uptake to aerosol, which is then measured as enhancements in pNO_3. N_2O was another species which sometimes posed challenges to the estimation of NEMRs. For some diffuse plumes, such as Rattlesnake Creek RF01, N_2O was not clearly enhanced above background levels. N_2O is long-lived in the troposphere and has a relatively high background (∼330 ppbv). Given expected emission factors (Akagi et al., 2011) of 0.16 g kg^{-1} for N_2O and 89 g kg^{-1} CO for temperate forests, we should only expect to see ∼1 ppbv enhancement in N_2O in plumes with maximum CO < 1,000 ppbv. This is close to the estimated uncertainty in the N_2O measurement (±1 ppbv). Examples of the timeseries of N_2O, CO, NH_3, and CO_2 for four examples of different density plumes are included in the supplement to show differences between species with generally large enhancements relative to background (e.g., CO and NH_3) and species with relatively smaller enhancements relative to background (e.g., N_2O and CO_2) (Figures S4–S7). We only report N_2O NEMRs for transects where N_2O is positively correlated with CO with $R^2 > 0.5$. This may bias the results toward plumes with either larger absolute N_2O emissions or favorable background conditions, but ensures that we do not present N_2O NEMRs that are not physical (i.e., negative values) and therefore artificially low.

Taken together, Figures 2a and 2b indicate significant variability in total observed N_r enhancements and their distribution across N_r species. This variability could be attributed to fire-to-fire differences in N_r emissions, as well as differences in the chemical aging of each plume. Several lab studies have confirmed the influence of both burn conditions and fuel N on the emissions of N_r. (Burling et al., 2010; Coggon et al., 2016; Roberts et al., 2020). Fire characteristics such as burn temperature, geometry, fuel moisture, and combustion efficiency will all impact the total quantity of N_r in smoke if they change the fraction of fuel N released; these factors can also strongly affect the distribution of the N_r. However, the WE-CAN observations of large wildfires do not provide a constraint on the fuel N content or the total amount volatilized. A large fraction of fuel N is released as N_2 (e.g., Kuhlbusch et al., 1991) and some fraction of fuel N remains in the ash after burning (e.g., Yokelson et al., 1996). In situ N_2 measurements were not attempted during WE-CAN (and would not likely be precise enough to quantify denitrification of fuel N to N_2), and accurate ground measurements of fuel- and ash- N content of each fire at the time of sampling are not available.

We do not observe significant variability in total observed ΣN_r enhancements between emission transects on the same fires sampled over multiple 30 min periods during the same flight (fire names with a, b, or c after them in Figure 2a). The relative distribution of N_r species is also similar across these pairs or triplet sets of emissions transects. In other words, over short time periods (30 min to several hours during afternoon/early evening) we are not able to discern whether these fires are changing quickly with respect to the amount or distribution of N_r they emit.

3.2. N_r Distribution Dependencies

Previous research has explored the relationship between combustion efficiency and other metrics of burn conditions, and the ratio of reduced to oxidized N_r in wildfire smoke (e.g., Goode et al., 1999; McMeek-
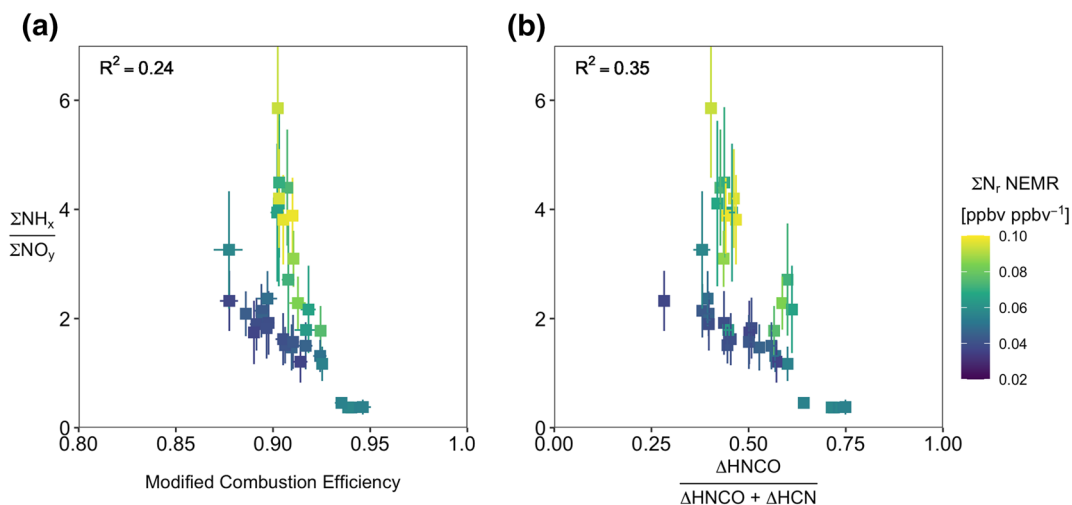
Figure 3. Relationships between the ratio of ΣNH_x ($= NH_3 + pNH_4$) to ΣNO_y with: (a) MCE, and (b) the fraction of HCN + HNCO that exists as HNCO.

ing et al., 2009). As noted in the introduction, the MCE can reflect different mixtures of fire processes that produce N_r emissions, with a lower MCE fire expected to produce more NH_3, and a higher MCE fire expected to produce more NO_x. Figure 3a presents a scatter plot of the molar ratio of $\Sigma NH_x/\Sigma NO_y$, where $\Sigma NH_x = NH_3 + pNH_4$ and ΣNO_y = sum of measured oxidized N species. We display this ratio instead of NH_3/NO_x (Figure S8) to account for chemical evolution in the time since emission. WE-CAN emission transects display a weak negative relationship between this ratio and MCE ($R^2 = 0.24$). This negative relationship is expected given past studies have found similar negative relationships in lab and field data, though the variance explained by MCE in past studies has sometimes been higher. For example, in both boreal wildfires and savannah grass fires, Goode et al. (1999, 2000) found that the ratio of NH_3/NO_x had a strong negative relationship with MCE ($R^2 = 0.94$). They found that the NH_3/NO_x ratio in both boreal and savannah plumes falls along the same linear regression line of MCE. However, McMeeking et al. (2009) show with additional lab and field data that the ratio of NH_3/NO_x is not always strongly anti-correlated with MCE, and does not always follow the same linear regression. The WE-CAN data similarly show that while MCE may explain the general pattern in the $\Sigma NH_x/\Sigma NO_y$ ratio observed for large daytime western U.S. wildfires, other factors contribute to the variability in this ratio as well. For instance, the colorbar in Figure 3 indicates that the total amount of measured ΣN_r has a positive correlation with the $\Sigma NH_x/\Sigma NO_y$ ratio. That is, the more N_r emitted by the fire, the more NH_3 we might expect to be present relative to NO_x. The relationship of $\Sigma NH_x/\Sigma NO_y$ with ΣN_r itself has a $R^2 = 0.43$, with ΣN_r explaining roughly the same amount of the variance in $\Sigma NH_x/\Sigma NO_y$ as MCE (shown in Figure S9). The measured ΣN_r likely contains information about the fuel N content combined with how much fuel N was volatilized, complicated by how much of the volatilized N_r was denitrified to N_2.

Given our understanding of the initial pyrolysis of fuel N, holding denitrification ($N_r \rightarrow N_2$) reactions constant, we would expect a higher observed total ΣN_r to reflect a higher amount of fuel N volatilized. A higher amount of fuel N volatilized would manifest as increased amounts of N in small reduced forms (NH_3, HCN, HNCO). In the flame chemistry following the initial volatilization, some portion of these more reduced forms are oxidized to NO_x and HONO. The MCE likely reflects the combustion temperatures, with higher MCE and higher temperatures leading to more complete oxidation and vice versa. Combustion temperatures are also likely linked to the amount of denitrification that takes place. With higher combustion temperatures we would expect more denitrification. This would be a different reason for measured ΣN_r to be smaller at higher MCE. The pattern in the coloration of Figure 3 is consistent with contributions from each of these three linked processes. There is a higher $\Sigma NH_x/\Sigma NO_y$ ratio at lower MCE points, and when the total observed ΣN_r is higher at a given MCE, this ratio also increases. Therefore,

the variability in the ratio of $\Sigma NH_x/\Sigma NO_y$ is likely influenced by both burn conditions and the total fuel N volatilized.

We also compare the fraction of HNCO in the sum of HNCO and HCN to the ratio of $\Sigma NH_x/\Sigma NO_y$ in Figure 3b. We hypothesize that the ratio of $\Sigma NH_x/\Sigma NO_y$ will have a tighter correlation with the fraction of HNCO than MCE because emissions of HNCO and HCN have been shown to have a temperature dependence (Hansson et al., 2004; Roberts et al., 2020), and are directly influenced by the amount of fuel N (Coggon et al., 2016). We do indeed find a weak negative relationship, shown in Figure 3b, with lower $\Sigma NH_x/\Sigma NO_y$ ratios at higher HNCO fractions (and higher assumed combustion temperatures). However, this negative relationship ($R^2 = 0.35$) is not much stronger than that with MCE, and so our hypothesis that the HNCO fraction would have a more clear relationship with other N_r species is not supported. This may be because both HCN and HNCO can be oxidized to other species (NO_x, HONO etc.) and we should expect more oxidation with increasing combustion temperature. If this oxidation affects HCN and HNCO somewhat differently, then it may be able to change the relationship of HNCO/HCN and combustion temperature.

In summary, the similarity between both the $\Sigma NH_x/\Sigma NO_y$ relationship with both the HNCO fraction and with MCE suggests that combustion conditions and processes are driving some of the variability in the distribution of N_r in WE-CAN fires. Likewise, a similar amount of variability in $\Sigma NH_x/\Sigma NO_y$ explained by ΣN_r suggests that more N_r survives denitrification reactions at lower MCEs, and that the amount of fuel N volatilized may also contribute to the observed differences in $\Sigma NH_x/\Sigma NO_y$ across fires. These variables explain a larger fraction of the variability in $\Sigma NH_x/\Sigma NO_y$ than in NH_3/NO_x since $\Sigma NH_x/\Sigma NO_y$ accounts for much of the possible chemical evolution between emission and sampling (Figures 3 and S9). Other in situ data or metrics for specific fire characteristics such as burn temperature, burn geometry, and fuel moisture content are difficult to gather for complex wildfires like those sampled during WE-CAN. Attempts to relate satellite-derived fire radiative power estimates during the time of sampling to the ratio of $\Sigma NH_x/\Sigma NO_y$ do not yield any relationships (Figure S10a). Likewise, predicted 1,000-h fuel moisture at the time of the burn from GRIDMET (Abatzoglou, 2011) (www.climatologylab.org/gridmet.html) is not correlated with the ratio of $\Sigma NH_x/\Sigma NO_y$ (Figure S10b).

Recent measurements of NVOCs in smoke have been made in laboratory burns (e.g., Gilman et al., 2015; Koss et al., 2018; Stockwell et al., 2015) and in the field (e.g., Coggon et al., 2016; Liu et al., 2017; this study) via Proton-Transfer-Reaction Mass Spectrometry and chemical ionization time-of-flight mass spectrometry. NVOC EFs have been shown to depend on MCE (Coggon et al., 2016) and may be important for the formation of brown carbon and toxicity of wildfire smoke (Koss et al., 2018). In Figure S11, we show the calculated EFs of measured NVOCs summed over amide-, amine-, N-heterocyclic-, nitrile- (excluding CH_3CN), and nitroalkane-groups quantified for WE-CAN emissions transects, plotted against MCE. We observe negative correlations with MCE for all groups except the nitroalkanes.

3.3. Comparison to Laboratory Studies

We now compare WE-CAN field estimates of N_r emission factors to those measured in laboratory settings for similar fuel types. Several experiments have previously measured emissions from controlled burns of myriad fuel types in laboratories such as the Missoula Fire Lab. These emission factors are used to inform fire emission inputs into regional and global chemical transport models.

Using our calculated in situ emission factors, we match lab emission factors from specific fuel types to WE-CAN fires that included the same fuel type. Since all fires sampled by WE-CAN contained complex mixtures of fuels, estimates of the percentage of each fuel type burned are provided by the U.S. Forest Service. Most fires contained >5 fuel types contributing significant percentages to the overall area burned. Since we don't have a precise estimate of exactly which fuel(s) contributed to the smoke we sampled on a given fire, we include any fuel type with >10% contribution to the overall fuel burned for a given fire in this comparison. For example, several burns of ponderosa pine fuels were tested during the FIREX 2016 lab study (Selimovic et al., 2018), and any WE-CAN fire with >10% contribution from ponderosa pine is included in the comparison to those FIREX 2016 lab ponderosa pine burns. In this way, the same WE-CAN fire may be compared to several different specific fuel types burned in the lab.
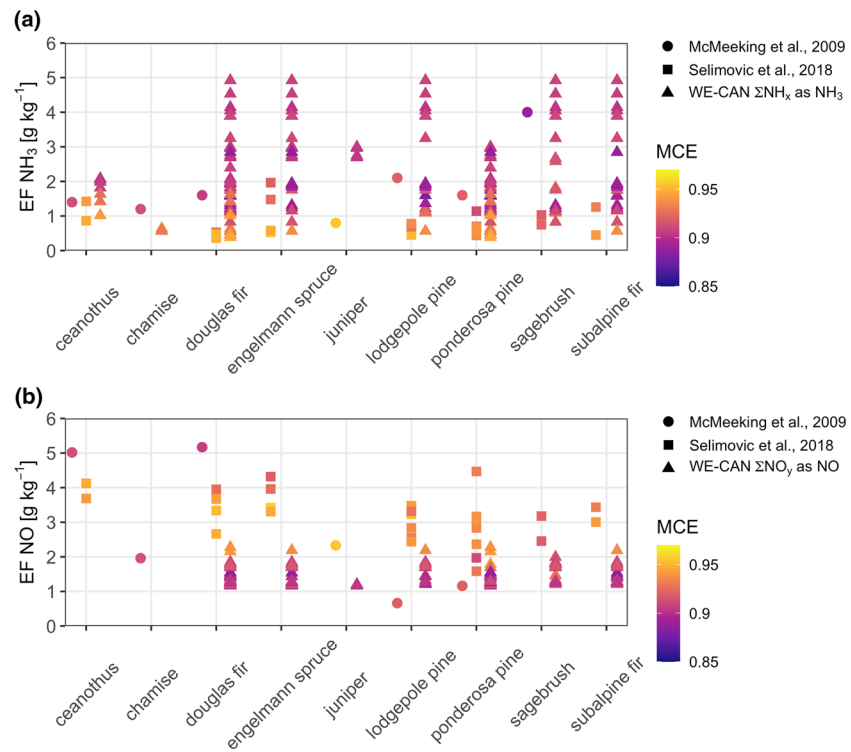
Figure 4. Comparison between WE-CAN ΣNH_x and ΣNO_y emission factors to NH_3 and NO_x emission factors from FLAME-2 and FIREX-2016 lab studies. Colors indicate MCE.

Figure 4 shows the results of this comparison for NH_3 and NO_x with EFs from the FLAME-2 (McMeeking et al., 2009) and FIREX-2016 (Selimovic et al., 2018) laboratory studies. Both experiments burned a range of fuels and fuel types from across the western U.S. in the U.S. Forest Service Missoula Fire Sciences Laboratory. Here we again use WE-CAN ΣNH_x and ΣNO_y as proxies for NH_3 and NO_x at emission. We find that ΣNH_x EFs during WE-CAN for fires burning the same fuels as those burned in the lab are similar to or of a larger magnitude than the NH_3 lab EFs. Conversely, ΣNO_y EFs from WE-CAN are generally lower than NO_x EFs from the lab. Each emission factor is also colored by the burn average or emissions transect MCE. These sets of lab experiments largely represent higher MCEs than the WE-CAN data, but that is, not always the case. Figure 4 indicates that WE-CAN EFs associated with higher MCEs are more closely
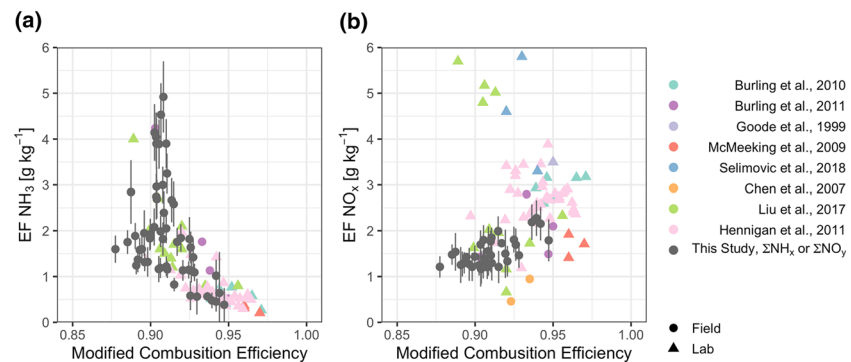

Figure 5. Comparison of (a) NH_3 and (b) NO_x emissions factor relationships with MCE. WE-CAN data are in black with propagated uncertainties shown as vertical errorbars, and literature data colored by study and with different shapes reflecting lab (triangle) or field measurements (circle) (literature data accessed from the SERA database: https://depts.washington.edu/nwfire/sera/).
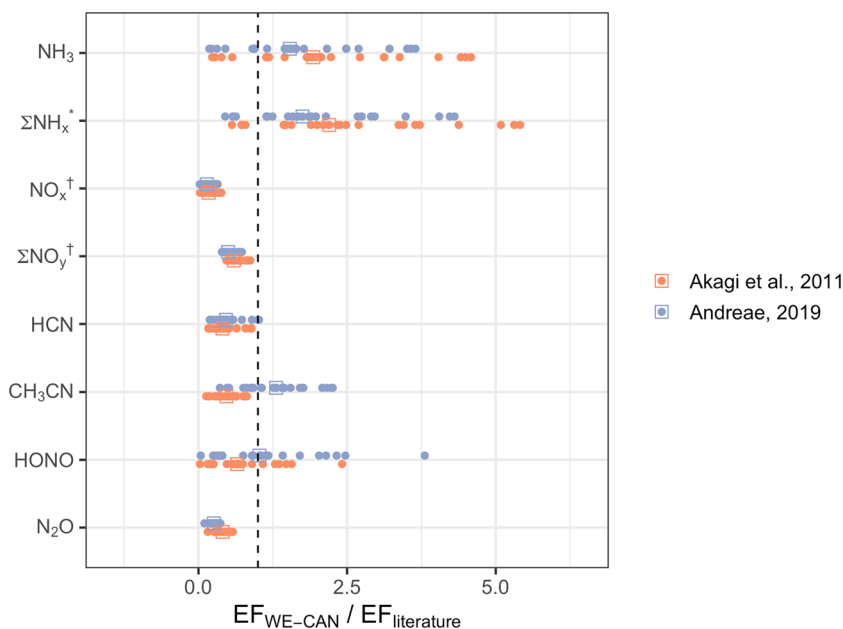
Figure 6. Comparison between the ratio of different WE-CAN N_r EFs and the best estimate temperate forest EF for the same compound compiled in Akagi et al. (2011) (red dots) and Andreae (2019) (blue dots) for use in models. Square points indicate the median ratio across all WE-CAN emission transect estimates. * $EF_{WE\text{-}CAN}$ ΣNH_x is compared to the NH_3 $EF_{literature}$. † $EF_{WE\text{-}CAN}$ NO_x and ΣNO_y are compared to NO $EF_{literature}$.

comparable to the lab studies. Figure 5 shows the relationship between EFs and MCE across a wider range of previous studies applicable to western U.S. wildfires, without sorting by fuel type. We note that the error associated with our EF estimates is large, typically on the order of 30%–40%. These same errors are applicable to Figures 4 and 6 as well, but displaying them would complicate the ease of understanding these figures. While the differences in burn conditions as captured by MCE between field and lab may offer one explanation for the difference between WE-CAN ΣNH_x and ΣNO_y EFs and the lab, another possible explanation for oxidized N is missing or uncertain NO_y measurements. The quantification of multifunctional organic nitrates and other oxidized N-containing NVOCs in the WE-CAN dataset is very uncertain. If these are present in higher quantities than we have estimated in smoke, and were directly or indirectly formed via reactions involving NO_x, then we could still underestimate the EFs of NO_x from WE-CAN by using the ΣNO_y EFs.

We can also compare EFs from WE-CAN to those compiled in the literature for use in models by Akagi et al. (2011) and Andreae (2019) (Figure 6). Akagi et al. (2011) and Andreae (2019) both report EF factors for broad vegetation types with extratropical forest split between temperate and boreal forests. Since our fire locations were all within the lower 48 U.S. states, here we compare all WE-CAN EFs to their respective "Temperate Forest" best estimates. Figure 6 displays the ratio of WE-CAN emission factors for each transect to these literature best estimate values for temperate forests, with values greater than one indicating a WE-CAN transect EF estimate larger than that value and vice versa. The square points identify the median value across all of the WE-CAN emission transect estimates. Consistent with the previous comparisons, we find WE-CAN NH_3 and ΣNH_x EFs to be generally larger than the literature compilations, while NO_x and ΣNO_y EFs to be smaller. HCN, N_2O, and HONO EFs are also smaller, with large variability in the HONO emission factors (see Peng et al., 2020, for more information), and CH_3CN is smaller than Akagi et al. (2011), and about the same as Andreae (2019). In our final comparison with laboratory measurements, we compare the NVOC EF estimates to the lab burn measurements of Koss et al. (2018) for nine species measured in common (Figure S12). We find general agreement in magnitude and the negative correlation between each NVOC and MCE between this study and Koss et al. (2018), though we note that the MCEs observed by Koss et al. (2018) were on average higher than those observed here.

4. Summary and Conclusions

The WE-CAN field campaign sampled smoke from 23 wildfires across the western U.S. during summer 2018. WE-CAN sampled fires of various sizes; most fires exceeded 1,000 acres, and the eventual total burn area of several fires sampled during the WE-CAN campaign exceeded 100,000 acres. Sampling was conducted from the mid-afternoon to early evening period. This means wildfires were primarily sampled during periods with well-developed vertical plumes, often during periods of rapid fire spread. We present NEMRs and EFs for a suite of N_r species calculated using these measurements. The three main conclusions from this work as are follows:

1. We observe that reduced N species account for between 39% and 80% (median = 66%) of the total measured ΣN_r in fresh smoke plumes. Gas-phase NH_3 accounts for the majority of the reduced N, with smaller contributions from pNH$_4$, HCN, and HNCO. The largest contributors to oxidized N are NO_x, pNO$_3$, ΣONs, HONO, and PAN. As the primary WE-CAN sampling strategy was focused on large fires during periods with flaming fronts during mid-afternoon conditions, prior work might imply that oxidized N_r emissions (largely from flaming combustion) should dominate the total measured ΣN_r. However, that is not what the WE-CAN data show.
2. Within minutes after emission, rapid chemistry occurs that changes the distribution (species/amount/phase) of N_r in fresh smoke plume. Due to this rapid chemistry, we compare total ΣNO_y and measured ΣNH_x with common metrics of fire characteristics, such as MCE, rather than NO_x and NH_3 by themselves. The ratio of $\Sigma NH_x / \Sigma NO_y$ generally decreases with increasing MCE, qualitatively consistent with previous research, and a similar relationship between $\Sigma NH_x / \Sigma NO_y$ and the HNCO fraction further suggest that combustion process and conditions drive some of the variability in the distribution of N_r between reduced and oxidized forms. Through the negative correlation between $\Sigma NH_x / \Sigma NO_y$ and the total measured ΣN_r, we propose that fuel N content/volatilization differences between fires may also contribute to the observed variability in $\Sigma NH_x / \Sigma NO_y$, though this interpretation is complicated somewhat by unquantifiable influence from denitrification reactions ($N_r \rightarrow N_2$) that are likely more prevalent under more flaming combustion conditions.
3. For similar fuel types the ΣNH_x EFs are of the same magnitude or larger than lab-based NH_3 EFs, whereas ΣNO_y EFs are on average smaller than lab-based NO_x EFs. One possible explanation for the difference in ΣNO_y compared to lab NO_x is differences in the burn conditions between field and lab. WE-CAN sampled fires with MCEs between the median and lower limit of fires sampled previously and while WE-CAN EF estimates contain larger variability, the agreement with lab studies for ΣNH_x and NH_3 EFs is better when only comparing across similar MCEs. Uncertain quantification of multifunctional organic nitrates and missing quantification of additional oxidized N-containing NVOCs in the WE-CAN dataset may be another possible reason for this difference. If we consider all fuels sampled to be classified as temperate forest, we can also compare WE-CAN EFs to literature compilations of EFs for use in models.

In future work, we will connect these N_r emissions to chemical processes and aging that occurs further downwind. While WE-CAN was able to sample a large number and variety of fires throughout the western U.S., this dataset is biased toward large, afternoon fires with smoke plumes lofted into the free troposphere. This analysis may not be applicable to estimates of N_r emissions from fires at different times of day and stages of growth. Data from several other recent field campaigns that have sampled smoke will be helpful in further refining our knowledge of emission of N_r from western U.S. wildfires.

Data Availability Statement

All data are available in the WE-CAN data archive (https://data.eol.ucar.edu/master_lists/generated/we-can/). The authors declare no conflicts of interest.

References

Abatzoglou, J. T. (2011). Development of gridded surface meteorological data for ecological applications and modelling. *International Journal of Climatology*, *33*(1), 121–131. https://doi.org/10.1002/joc.3413

Akagi, S. K., Craven, J. S., Taylor, J. W., McMeeking, G. R., Yokelson, R. J., Burling, I. R., et al. (2012). Evolution of trace gases and particles emitted by a chaparral fire in California. *Atmospheric Chemistry and Physics*, *12*(3), 1397–1421. https://doi.org/10.5194/acp-12-1397-2012

Akagi, S. K., Yokelson, R. J., Wiedinmyer, C., Alvarado, M. J., Reid, J. S., Karl, T., et al. (2011). Emission factors for open and domestic biomass burning for use in atmospheric models. *Atmospheric Chemistry and Physics*, *11*(9), 4039–4072. https://doi.org/10.5194/acp-11-4039-2011

Alvarado, M. J., Logan, J. A., Mao, J., Apel, E., Riemer, D., Blake, D., et al. (2010). Nitrogen oxides and PAN in plumes from boreal fires during ARCTAS-B and their impact on ozone: An integrated analysis of aircraft and satellite observations. *Atmospheric Chemistry and Physics*, *10*(20), 9739–9760. https://doi.org/10.5194/acp-10-9739-2010

Andreae, M. O. (2019). Emission of trace gases and aerosols from biomass burning–an updated assessment. *Atmospheric Chemistry and Physics*, *19*(13), 8523–8546. https://doi.org/10.5194/acp-19-8523-2019

Andrews, S. J., Carpenter, L. J., Apel, E. C., Atlas, E., Donets, V., Hopkins, J. R., et al. (2016). A comparison of very short lived halocarbon (VSLS) and DMS aircraft measurements in the tropical west Pacific from CAST, ATTREX and CONTRAST. *Atmospheric Measurement Techniques*, *9*(10), 5213–5225. https://doi.org/10.5194/amt-9-5213-2016

Bahreini, R., Dunlea, E. J., Matthew, B. M., Simons, C., Docherty, K. S., DeCarlo, P. F., et al. (2008). Design and operation of a pressure-controlled inlet for airborne sampling with an aerodynamic aerosol lens. *Aerosol Science and Technology*, *42*(6), 465–471. https://doi.org/10.1080/02786820802178514

Bahreini, R., Ervens, B., Middlebrook, A. M., Warneke, C., de Gouw, J. A., DeCarlo, P. F., et al. (2009). Organic aerosol formation in urban and industrial plumes near Houston and Dallas, Texas. *Journal of Geophysical Research*, *114*, http://dx.doi.org/10.1029/2008jd011493

Benedict, K. B., Zhou, Y., Sive, B. C., Prenni, A. J., Gebhart, K. A., Fischer, E. V., et al. (2019). Volatile organic compounds and ozone in rocky mountain national Park during FRAPPÉ. *Atmospheric Chemistry and Physics*, *19*(1), 499–521. https://doi.org/10.5194/acp-19-499-2019

Burling, I. R., Yokelson, R. J., Griffith, D. W. T., Johnson, T. J., Veres, P., Roberts, J. M., et al. (2010). Laboratory measurements of trace gas emissions from biomass burning of fuel types from the southeastern and southwestern United States. *Atmospheric Chemistry and Physics*, *10*(22), 11115–11130. https://doi.org/10.5194/acp-10-11115-2010

Chen, X., Day, D., Schichtel, B., Malm, W., Matzoll, A. K., Mojica, J., et al. (2014). Seasonal ambient ammonia and ammonium concentrations in a pilot IMPROVE NHx monitoring network in the western United States. *Atmospheric Environment*, *91*, 118–126. https://doi.org/10.1016/j.atmosenv.2014.03.058

Chen, L.-W. A., Verburg, P., Shackelford, A., Zhu, D., Susfalk, R., Chow, J. C., et al. (2010). Moisture effects on carbon and nitrogen emission from burning of wildland biomass. *Atmospheric Chemistry and Physics*, *10*(14), 6617–6625. https://doi.org/10.5194/acp-10-6617-2010

Coggon, M. M., Veres, P. R., Yuan, B., Koss, A., Warneke, C., Gilman, J. B., et al. (2016). Emissions of nitrogen-containing organic compounds from the burning of herbaceous and arboraceous biomass: Fuel composition dependence and the variability of commonly used nitrile tracers. *Geophysical Research Letters*, *43*(18), 9903–9912. https://doi.org/10.1002/2016GL070562

DeCarlo, P. F., Kimmel, J. R., Trimborn, A., Northway, M. J., Jayne, J. T., Aiken, A. C., et al. (2006). Field-deployable, high-resolution, time-of-flight aerosol mass spectrometer. *Analytical Chemistry*, *78*(24), 8281–8289. https://doi.org/10.1021/ac061249n

Farmer, D. K., Matsunaga, A., Docherty, K. S., Surratt, J. D., Seinfeld, J. H., Ziemann, P. J., et al. (2010). Response of an aerosol mass spectrometer to organonitrates and organosulfates and implications for atmospheric chemistry. *Proceedings of the National Academy of Sciences*, *107*(15), 6670–6675. https://doi.org/10.1073/pnas.0912340107

Garofalo, L. A., Pothier, M. A., Levin, E. J. T., Campos, T., Kreidenweis, S. M., & Farmer, D. K. (2019). Emission and evolution of submicron organic aerosol in smoke from wildfires in the western United States. *ACS Earth and Space Chemistry*, *3*(7), 1237–1247. https://doi.org/10.1021/acsearthspacechem.9b00125

Gilman, J. B., Lerner, B. M., Kuster, W. C., Goldan, P. D., Warneke, C., Veres, P. R., et al. (2015). Biomass burning emissions and potential air quality impacts of volatile organic compounds and other trace gases from fuels common in the US. *Atmospheric Chemistry and Physics*, *15*(24), 13915–13938. https://doi.org/10.5194/acp-15-13915-2015

Glarborg, P., Miller, J. A., Ruscic, B., & Klippenstein, S. J. (2018). Modeling nitrogen chemistry in combustion. *Progress in Energy and Combustion Science*, *67*, 31–68. https://doi.org/10.1016/j.pecs.2018.01.002

Goode, J. G., Yokelson, R. J., Susott, R. A., & Ward, D. E. (1999). Trace gas emissions from laboratory biomass fires measured by open-path Fourier transform infrared spectroscopy: Fires in grass and surface fuels. *Journal of Geophysical Research*, *104*(D17), 21237–21245. https://doi.org/10.1029/1999JD900360

Goode, J. G., Yokelson, R. J., Ward, D. E., Susott, R. A., Babbitt, R. E., Davies, M. A., et al. (2000). Measurements of excess O_3, CO_2, CO, CH_4, C_2H_4, C_2H_2, HCN, NO, NH_3, HCOOH, CH_3COOH, HCHO, and CH_3OH in 1997 Alaskan biomass burning plumes by airborne Fourier transform infrared spectroscopy (AFTIR). *Journal of Geophysical Research*, *105*(D17), 22147–22166. https://doi.org/10.1029/2000JD900287

Hansson, K.-M., Samuelsson, J., Tullin, C., & Åmand, L.-E. (2004). Formation of HNCO, HCN, and NH_3 from the pyrolysis of bark and nitrogen-containing model compounds. *Combustion and Flame*, *137*(3), 265–277. https://doi.org/10.1016/j.combustflame.2004.01.005

Hoover, K., & Hanson, L. A. (2019). National Interagency Fire Center Wildfire Statistics, (Vol. 2). Washington, DC: Congressional Research Service. https://fas.org/sgp/crs/misc/IF10244.pdf

Jaffe, D., Chand, D., Hafner, W., Westerling, A., & Spracklen, D. (2008). Influence of fires on O3 concentrations in the western US. *Environmental Science & Technology*, *42*(16), 5885–5891. https://doi.org/10.1021/es800084k

Jaffe, D. A., & Wigder, N. L. (2012). Ozone production from wildfires: A critical review. *Atmospheric Environment*, *51*, 1–10. https://doi.org/10.1016/j.atmosenv.2011.11.063

Kolden, C. A. (2019). We're not doing enough prescribed fire in the western United States to mitigate wildfire risk. *Fire*, *2*(2), 30. https://doi.org/10.3390/fire2020030

Koss, A. R., Sekimoto, K., Gilman, J. B., Selimovic, V., Coggon, M. M., Zarzana, K. J., et al. (2018). Non-methane organic gas emissions from biomass burning: Identification, quantification, and emission factors from PTR-ToF during the FIREX 2016 laboratory experiment. *Atmospheric Chemistry and Physics*, *18*(5), 3299–3319. https://doi.org/10.5194/acp-18-3299-2018

Kuhlbusch, T. A., Lobert, J. M., Crutzen, P. J., & Warneck, P. (1991). Molecular nitrogen emissions from denitrification during biomass burning. *Nature*, *351*(6322), 135–137. https://doi.org/10.1038/351135a0

Lebegue, B., Schmidt, M., Ramonet, M., Wastine, B., Yver Kwok, C., Laurent, O., et al. (2016). Comparison of nitrous oxide (N_2O) analyzers for high-precision measurements of atmospheric mole fractions. *Atmospheric Measurement Techniques*, *9*(3), 1221–1238. https://doi.org/10.5194/amt-9-1221-2016

Lee, B. H., Lopez-Hilfiker, F. D., Mohr, C., Kurtén, T., Worsnop, D. R., & Thornton, J. A. (2014). An iodide-adduct high-resolution time-of-flight chemical-ionization mass spectrometer: Application to atmospheric inorganic and organic compounds. *Environmental Science & Technology*, *48*(11), 6309–6317. https://doi.org/10.1021/es500362a

Lee, B. H., Lopez-Hilfiker, F. D., Veres, P. R., McDuffie, E. E., Fibiger, D. L., Sparks, T. L., et al. (2018). Flight deployment of a high-resolution time-of-flight chemical ionization mass spectrometer: Observations of reactive Halogen and nitrogen oxide species. *Journal of Geophysical Research: Atmospheres*, *123*(14), 7670–7686. https://doi.org/10.1029/2017JD028082

Lee, B. H., Mohr, C., Lopez-Hilfiker, F. D., Lutz, A., Hallquist, M., Lee, L., et al. (2016). Highly functionalized organic nitrates in the southeast United States: Contribution to secondary organic aerosol and reactive nitrogen budgets. *Proceedings of the National Academy of Sciences*, *113*(6), 1516–1521. https://doi.org/10.1073/pnas.1508108113

Lin, P., Aiona, P. K., Li, Y., Shiraiwa, M., Laskin, J., Nizkorodov, S. A., et al. (2016). Molecular characterization of Brown carbon in biomass burning aerosol particles. *Environmental Science & Technology*, *50*(21), 11815–11824. https://doi.org/10.1021/acs.est.6b03024

Liu, X., Huey, L. G., Yokelson, R. J., Selimovic, V., Simpson, I. J., Müller, M., et al. (2017). Airborne measurements of western U.S. wildfire emissions: Comparison with prescribed burning and air quality implications. *Journal of Geophysical Research: Atmospheres*, *122*(11), 6108–6129. https://doi.org/10.1002/2016JD026315

Liu, X., Zhang, Y., Huey, L. G., Yokelson, R. J., Wang, Y., Jimenez, J. L., et al. (2016). Agricultural fires in the southeastern U.S. during SEAC4RS: Emissions of trace gases and particles and evolution of ozone, reactive nitrogen, and organic aerosol. *Journal of Geophysical Research: Atmospheres*, *121*(12), 7383–7414. https://doi.org/10.1002/2016JD025040

Lobert, J. M., Scharffe, D. H., Hao, W. M., & Crutzen, P. J. (1990). Importance of biomass burning in the atmospheric budgets of nitrogen-containing gases. *Nature*, *346*(6284), 552–554. https://doi.org/10.1038/346552a0

Lobert, J. M., & Warnatz, J. (1993). Emissions from the combustion process in vegetation. In P. J. Crutzen, & J. G. Goldhammer (Eds.), *Fire in the environment: The ecological, atmospheric and climatic importance of vegetation fires*. New York, NY: John Wiley and Sons.

McAllister, S. (2019). The Role of Fuel Bed Geometry and Wind on the Burning Rate of Porous Fuels. *Frontiers in Mechanical Engineering*, *5*, https://doi.org/10.3389/fmech.2019.00011

McClure, C. D., & Jaffe, D. A. (2018). US particulate matter air quality improves except in wildfire-prone areas. *Proceedings of the National Academy of Sciences*, *115*(31), 7901–7906. https://doi.org/10.1073/pnas.1804353115

McManus, J. B., Kebabian, P. L., & Zahniser, M. S. (1995). Astigmatic mirror multipass absorption cells for long-path-length spectroscopy. *Applied Optics*, *34*(18), 3336–3348. https://doi.org/10.1364/AO.34.003336

McManus, J. B., Shorter, J. H., Nelson, D. D., & Zahniser, M. S. (2007). Compact quantum cascade laser instrument for rapid, high sensitivity measurements of trace gases in air. In *IEEE SENSORS* (pp. 1341–1344). https://doi.org/10.1109/ICSENS.2007.4388659

McManus, J. B., Zahniser, M. S., Jr, D. D. N., Shorter, J. H., Herndon, S. C., Wood, E. C., et al. (2010). Application of quantum cascade lasers to high-precision atmospheric trace gas measurements. *Optical Engineering*, *49*(11), 111124. https://doi.org/10.1117/1.3498782

McMeeking, G. R., Kreidenweis, S. M., Baker, S., Carrico, C. M., Chow, J. C., Collett, J. L., et al. (2009). Emissions of trace gases and aerosols during the open combustion of biomass in the laboratory. *Journal of Geophysical Research*, *114*(D19). http://dx.doi.org/10.1029/2009jd011836

Ottmar, R. D., Sandberg, D. V., Riccardi, C. L., & Prichard, S. J. (2007). An overview of the Fuel Characteristic Classification System—Quantifying, classifying, and creating fuelbeds for resource planning. *Canadian Journal of Forest Research*, *37*(12), 2383–2393. https://doi.org/10.1139/X07-077

O'Dell, K., Ford, B., Fischer, E. V., & Pierce, J. R. (2019). Contribution of wildland-fire smoke to US PM2.5 and its influence on recent trends. *Environmental Science & Technology*, *53*(4), 1797–1804. https://doi.org/10.1021/acs.est.8b05430

Palm, B. B., Liu, X., Jimenez, J. L., & Thornton, J. A. (2019). Performance of a new coaxial ion-molecule reaction region for low-pressure chemical ionization mass spectrometry with reduced instrument wall interactions. *Atmospheric Measurement Techniques*, *12*(11), 5829–5844. https://doi.org/10.5194/amt-12-5829-2019

Park, R. J., Jacob, D. J., Chin, M., & Martin, R. V. (2003). Sources of carbonaceous aerosols over the United States and implications for natural visibility. *Journal of Geophysical Research*, *108*(D12), 4355. https://doi.org/10.1029/2002JD003190

Park, R. J., Jacob, D. J., & Logan, J. A. (2007). Fire and biofuel contributions to annual mean aerosol mass concentrations in the United States. *Atmospheric Environment*, *41*(35), 7389–7400. https://doi.org/10.1016/j.atmosenv.2007.05.061

Peng, Q., Palm, B. B., Melander, K. E., Lee, B. H., Hall, S. R., Ullmann, K., et al. (2020). HONO emissions from western U.S. Wildfires provide dominant radical source in fresh wildfire smoke. *Environmental Science & Technology*, *54*(10), 5954–5963. https://doi.org/10.1021/acs.est.0c00126

Pollack, I. B., Lindaas, J., Roscioli, J. R., Agnese, M., Permar, W., Hu, L., et al. (2019). Evaluation of ambient ammonia measurements from a research aircraft using a closed-path QC-TILDAS operated with active continuous passivation. *Atmospheric Measurement Techniques*, *12*(7), 3717–3742. https://doi.org/10.5194/amt-12-3717-2019

Prenni, A. J., Levin, E. J. T., Benedict, K. B., Sullivan, A. P., Schurman, M. I., Gebhart, K. A., et al. (2014). Gas-phase reactive nitrogen near Grand Teton National Park: Impacts of transport, anthropogenic emissions, and biomass burning. *Atmospheric Environment*, *89*, 749–756. https://doi.org/10.1016/j.atmosenv.2014.03.017

Ren, Q., & Zhao, C. (2012). NOx and N_2O precursors from biomass pyrolysis: Nitrogen transformation from amino acid. *Environmental Science & Technology*, *46*(7), 4236–4240. https://doi.org/10.1021/es204142e

Ren, Q., & Zhao, C. (2013a). NOx and N_2O precursors from biomass pyrolysis: Role of cellulose, Hemicellulose and Lignin. *Environmental Science & Technology*, *47*(15), 8955–8961. https://doi.org/10.1021/es4017574

Ren, Q., & Zhao, C. (2013b). NOx and N_2O precursors (NH_3 and HCN) from biomass pyrolysis: Interaction between amino acid and mineral matter. *Applied Energy*, *112*, 170–174. https://doi.org/10.1016/j.apenergy.2013.05.061

Ridley, B. A., & Grahek, F. E. (1990). A small, low flow, high sensitivity reaction vessel for NO chemiluminescence detectors. *Journal of Atmospheric and Oceanic Technology*, *7*(2), 307–311. https://doi.org/10.1175/1520-0426(1990)007<0307:ASLFHS>2.0.CO;2

Ridley, B. A., Grahek, F. E., & Walega, J. G. (1992). A small high-sensitivity, medium-response ozone detector suitable for measurements from light aircraft. *Journal of Atmospheric and Oceanic Technology*, *9*(2), 142–148. https://doi.org/10.1175/1520-0426(1992)009<0142:ASHSMR>2.0.CO;2

Roberts, J. M., Stockwell, C. E., Yokelson, R. J., de Gouw, J., Liu, Y., Selimovic, V., et al. (2020). The nitrogen budget of laboratory-simulated western US wildfires during the FIREX 2016 Fire Lab study. *Atmospheric Chemistry and Physics*, *20*(14), 8807–8826. https://doi.org/10.5194/acp-20-8807-2020

Roberts, J. M., Veres, P., Warneke, C., Neuman, J. A., Washenfelder, R. A., Brown, S. S., et al. (2010). Measurement of HONO, HNCO, and other inorganic acids by negative-ion proton-transfer chemical-ionization mass spectrometry (NI-PT-CIMS): Application to biomass burning emissions. *Atmospheric Measurement Techniques*, *3*(4), 981–990. https://doi.org/10.5194/amt-3-981-2010

Rollins, M. G. (2009). LANDFIRE: A nationally consistent vegetation, wildland fire, and fuel assessment. *International Journal of Wildland Fire*, *18*(3), 235. https://doi.org/10.1071/WF08088

Russo, R. S., Zhou, Y., Haase, K. B., Wingenter, O. W., Frinak, E. K., Mao, H., et al. (2010). Temporal variability, sources, and sinks of C_1-C_5 alkyl nitrates in coastal New England. *Atmospheric Chemistry and Physics*, *10*(4), 1865–1883. https://doi.org/10.5194/acp-10-1865-2010

Russo, R. S., Zhou, Y., White, M. L., Mao, H., Talbot, R., & Sive, B. C. (2010). Multi-year (2004–2008) record of nonmethane hydrocarbons and halocarbons in new England: Seasonal variations and regional sources. *Atmospheric Chemistry and Physics*, *10*(10), 4909–4929. https://doi.org/10.5194/acp-10-4909-2010

Santín, C., Doerr, S. H., Preston, C. M., & González-Rodríguez, G. (2015). Pyrogenic organic matter production from wildfires: A missing sink in the global carbon cycle. *Global Change Biology*, *21*(4), 1621–1633. https://doi.org/10.1111/gcb.12800

Scharko, N. K., Oeck, A. M., Myers, T. L., Tonkyn, R. G., Banach, C. A., Baker, S. P., et al. (2019). Gas-phase pyrolysis products emitted by prescribed fires in pine forests with a shrub understory in the southeastern United States. *Atmospheric Chemistry and Physics*, *19*(15), 9681–9698. https://doi.org/10.5194/acp-19-9681-2019

Schoennagel, T., Balch, J. K., Brenkert-Smith, H., Dennison, P. E., Harvey, B. J., Krawchuk, M. A., et al. (2017). Adapt to more wildfire in western North American forests as climate changes. *Proceedings of the National Academy of Sciences*, *114*(18), 4582–4590. https://doi.org/10.1073/pnas.1617464114

Schultz, C. A., & Moseley, C. (2019). Collaborations and capacities to transform fire management. *Science*, *366*(6461), 38–40. https://doi.org/10.1126/science.aay3727

Sekimoto, K., Koss, A. R., Gilman, J. B., Selimovic, V., Coggon, M. M., Zarzana, K. J., et al. (2018). High- and low-temperature pyrolysis profiles describe volatile organic compound emissions from western US wildfire fuels. *Atmospheric Chemistry and Physics*, *18*(13), 9263–9281. https://doi.org/10.5194/acp-18-9263-2018

Sekimoto, K., Li, S.-M., Yuan, B., Koss, A., Coggon, M., Warneke, C., et al. (2017). Calculation of the sensitivity of proton-transfer-reaction mass spectrometry (PTR-MS) for organic trace gases using molecular properties. *International Journal of Mass Spectrometry*, *421*, 71–94. https://doi.org/10.1016/j.ijms.2017.04.006

Selimovic, V., Yokelson, R. J., Warneke, C., Roberts, J. M., de Gouw, J., Reardon, J., et al. (2018). Aerosol optical properties and trace gas emissions by PAX and OP-FTIR for laboratory-simulated western US wildfires during FIREX. *Atmospheric Chemistry and Physics*, *18*(4), 2929–2948. https://doi.org/10.5194/acp-18-2929-2018

Slusher, D. L., Huey, L. G., Tanner, D. J., Flocke, F. M., & Roberts, J. M. (2004). A thermal dissociation–chemical ionization mass spectrometry (TD-CIMS) technique for the simultaneous measurement of peroxyacyl nitrates and dinitrogen pentoxide. *Journal of Geophysical Research*, *109*(D19). https://doi.org/10.1029/2004jd004670

Stockwell, C. E., Veres, P. R., Williams, J., & Yokelson, R. J. (2015). Characterization of biomass burning emissions from cooking fires, peat, crop residue, and other fuels with high-resolution proton-transfer-reaction time-of-flight mass spectrometry. *Atmospheric Chemistry and Physics*, *15*(2), 845–865. https://doi.org/10.5194/acp-15-845-2015

Stockwell, C. E., Yokelson, R. J., Kreidenweis, S. M., Robinson, A. L., DeMott, P. J., Sullivan, R. C., et al. (2014). Trace gas emissions from combustion of peat, crop residue, domestic biofuels, grasses, and other fuels: Configuration and Fourier transform infrared (FTIR) component of the fourth fire lab at Missoula experiment (FLAME-4). *Atmospheric Chemistry and Physics*, *14*(18), 9727–9754. https://doi.org/10.5194/acp-14-9727-2014

Sullivan, A. P., Guo, H., Schroder, J. C., Campuzano-Jost, P., Jimenez, J. L., Campos, T., et al. (2019). Biomass burning markers and residential burning in the WINTER aircraft campaign. *Journal of Geophysical Research: Atmospheres*, *124*(3), 1846–1861. https://doi.org/10.1029/2017JD028153

Trentmann, J., Yokelson, R. J., Hobbs, P. V., Winterrath, T., Christian, T. J., Andreae, M. O., et al. (2005). An analysis of the chemical processes in the smoke plume from a savanna fire. *Journal of Geophysical Research*, *110*(D12). https://doi.org/10.1029/2004JD005628

Westerling, A. L. (2016). Increasing western US forest wildfire activity: sensitivity to changes in the timing of spring. *Philosophical Transactions of the Royal Society B: Biological Sciences*, *371*(1696), 20150178. https://doi.org/10.1098/rstb.2015.0178

Williams, A. P., Abatzoglou, J. T., Gershunov, A., Guzman-Morales, J., Bishop, D. A., Balch, J. K., et al. (2019). Observed impacts of anthropogenic climate change on wildfire in California. *Earth's Future*, *7*(8), 892–910. https://doi.org/10.1029/2019EF001210

Yokelson, R. J., Andreae, M. O., & Akagi, S. K. (2013a). Pitfalls with the use of enhancement ratios or normalized excess mixing ratios measured in plumes to characterize pollution sources and aging. *Atmospheric Measurement Techniques*, *6*(8), 2155–2158. https://doi.org/10.5194/amt-6-2155-2013

Yokelson, R. J., Burling, I. R., Gilman, J. B., Warneke, C., Stockwell, C. E., de Gouw, J., et al. (2013b). Coupling field and laboratory measurements to estimate the emission factors of identified and unidentified trace gases for prescribed fires. *Atmospheric Chemistry and Physics*, *13*(1), 89–116. https://doi.org/10.5194/acp-13-89-2013

Yokelson, R. J., Goode, J. G., Ward, D. E., Susott, R. A., Babbitt, R. E., Wade, D. D., et al. (1999). Emissions of formaldehyde, acetic acid, methanol, and other trace gases from biomass fires in North Carolina measured by airborne Fourier transform infrared spectroscopy. *Journal of Geophysical Research*, *104*(D23), 30109–30125. https://doi.org/10.1029/1999JD900817

Yokelson, R. J., Griffith, D. W. T., & Ward, D. E. (1996). Open-path Fourier transform infrared studies of large-scale laboratory biomass fires. *Journal of Geophysical Research*, *101*(D15), 21067–21080. https://doi.org/10.1029/96JD01800

Yokelson, R. J., Susott, R., Ward, D. E., Reardon, J., & Griffith, D. W. T. (1997). Emissions from smoldering combustion of biomass measured by open-path Fourier transform infrared spectroscopy. *Journal of Geophysical Research*, *102*(D15), 18865–18877. https://doi.org/10.1029/97JD00852

Yuan, B., Koss, A. R., Warneke, C., Coggon, M., Sekimoto, K., & de Gouw, J. A. (2017). Proton-transfer-reaction mass spectrometry: Applications in atmospheric Sciences. *Chemical Reviews*, *117*(21), 13187–13229. https://doi.org/10.1021/acs.chemrev.7b00325

Zahniser, M. S., Nelson, D. D., McManus, J. B., Kebabian, P. L., Lloyd, D., Fowler, D., et al. (1995). Measurement of trace gas fluxes using tunable diode laser spectroscopy. *Philosophical Transactions of the Royal Society of London. Series A: Physical and Engineering Sciences*, *351*(1696), 371–382. https://doi.org/10.1098/rsta.1995.0040

Zheng, W., Flocke, F. M., Tyndall, G. S., Swanson, A., Orlando, J. J., Roberts, J. M., et al. (2011). Characterization of a thermal decomposition chemical ionization mass spectrometer for the measurement of peroxy acyl nitrates (PANs) in the atmosphere. *Atmospheric Chemistry and Physics*, *11*(13), 6529–6547. https://doi.org/10.5194/acp-11-6529-2011

Zhou, Y., Shively, D., Mao, H., Russo, R. S., Pape, B., Mower, R. N., et al. (2010). Air toxic emissions from snowmobiles in Yellowstone National Park. *Environmental Science & Technology*, *44*(1), 222–228. https://doi.org/10.1021/es9018578